Revisiting the role of cAMP in Drosophila aversive olfactory memory formation

Takashi Abe[1†*], Daisuke Yamazaki[1†], Makoto Hiroi[1,2], Yutaro Ueoka[1], Yuko Maeyama[1] and Tetsuya Tabata[1*]

[1]Institute for Quantitative Biological Sciences, The University of Tokyo, Tokyo, Japan.

[2]Present address, Okinawa Institute of Science and Technology.

[†]These authors contributed equally to this work

[*]For Correspondence: tabe@iqb.u-tokyo.ac.jp (TA); ttabata@iqb.u-tokyo.ac.jp (TT)

Abstract

In the olfactory aversive conditioning of Drosophila melanogaster, an odor, the conditioned stimulus (CS), is associated with electric shock, the unconditioned stimulus (US). The Rutabaga adenylyl cyclase in Kenyon cells (KCs) of the fly brain synthesizes cAMP, which is believed to serve as the coincidence detector synergistically stimulated by calcium/calmodulin evoked by the odor reception and GαS released in response to the dopamine signaling elicited by electric shock. However, live imaging analyses revealed that olfactory stimulation itself prompted the activation of dopaminergic neurons and resulted in the elevation of cAMP levels in KCs that received dopamine, regardless of calcium signaling. This finding raises questions about the longstanding

and fundamental comprehension of conditioning mechanisms, as the cAMP levels in conditioned stimulus-positive (CS+) KCs could not be distinguished from those in the rest of the KCs. Our findings suggest that cAMP concentrations do not function as a mnemonic engram to CS+ neurons. Rather, the collective dynamics of cAMP are capable of integratively encoding the valence ascribed to odors being perceived at a given time. Furthermore, our investigation revealed that associative conditioning induces modifications in dopamine levels in response to both CS and US, resulting in alterations in cAMP levels. The increase in cAMP exerts a deleterious effect on the acetylcholine transmission from KCs. Accordingly, we postulate that, during conditioning, cAMP depresses KCs, thereby skewing the valence of the CS+ odor towards a more aversive state for the conditioned flies, and ultimately culminating in the formation of aversive memories.

Introduction

A quintessential aspect of classical conditioning involves the temporal pairing of an initially neutral stimulus, the conditioned stimulus (CS), with a reinforcing stimulus, the unconditioned stimulus (US), and the preservation of this association at the level of synaptic connections, leading to the manifestation of a conditioned response to the CS (Rescorla, 1988). The temporal correlation between the CS and US is mediated by coincidence detection mechanisms. One of the well-known coincidence detectors is adenylyl cyclase (AC), which is stimulated by both calcium/calmodulin and G-proteins coupled to receptors and catalyzes the conversion of ATP to cAMP. This was first revealed by the pioneering studies on classical conditioning of gill-withdrawal in the sea mollusca Aplysia. When siphon stimulation (CS) and electric shock to the tail (US) were repeatedly paired, the CS elicited potentiated gill- and siphon-withdrawal reflexes (Carew et al., 1981). Integration of the calcium influx resulting from the CS and the serotonin release resulting from the shock to the tail (US) increased the cAMP levels (Ocorr et al., 1985), as also shown biochemically (Abrams and Kandel, 1988; Yovell et al., 1992). These physiological and biochemical studies highlighted the pivotal role of adenylyl cyclase as a coincidence detector, which was strengthened by the genetic dissection of another model for the classical conditioning of Drosophila olfactory

memory (Abrams and Kandel, 1988; Levin et al., 1992; Livingstone et al., 1984; Tully, 1987; Tully and Quinn, 1985). Odor information via acetylcholine (ACh) signaling represents the CS (Gu and O'Dowd, 2006), and G-proteins coupled to dopamine metabotropic receptors (Kim et al., 2007) activated by dopaminergic neurons encode the US (electric shocks or sugar reward) in Drosophila (Burke et al., 2012; Liu et al., 2012; Riemensperger et al., 2005; Schwaerzel et al., 2003). These two input pathways converge on the Rutabaga adenylyl cyclase (AC) (Davis, 1993; Livingstone et al., 1984) expressed in Kenyon cells (KCs)(McGuire et al., 2003; Zars et al., 2000) of the mushroom bodies (MBs)(Heisenberg, 2003).

Genetically encoded fluorescent sensors have recently enabled the microscopic visualization of the dynamics of AC activities in fly brains. Tomchik and Davis showed the Rutabaga AC-dependent synergistic increase in cAMP in α/β and α'/β' KCs when acetylcholine (CS) and dopamine (US) application were paired to *ex vivo* brain explants (Tomchik and Davis, 2009). They also demonstrated that elevating cAMP acutely enhanced KC excitability. Additionally, Handler et al. reported a synergistic increase in cAMP levels in γ KCs upon temporal pairing of acetylcholine application with dopamine neuron activation in *ex vivo* brain explants (Handler et al., 2019). Gervasi et al. employed protein kinase A (PKA) activity as an indicator of cAMP

levels, and reported that the simultaneous administration of acetylcholine and dopamine led to an augmentation of PKA activity exclusively in α/β KCs, in a manner dependent on the Rutabaga AC (Gervasi et al., 2010). These findings collectively indicate that the Rutabaga AC fulfills its long-held role as a coincidence detector. It is worth noting, however, that these imaging experiments did not measure cAMP or PKA transients at a cellular resolution, but rather as a unit of the lobe, comprising a cluster of KC axons. It is estimated that, on average, roughly 5% of KCs exhibit a consistent response to monomolecular odors such as 3-octanol (OCT) and 4-methylcyclohexanol (MCH), as employed in these experiments (Honegger et al., 2011). This sparse nature of coding is essential for distinguishing a conditioned stimulus (CS+) odor from a non-conditioned stimulus (CS-) odor in classical conditioning. Thus, if the Rutabaga AC serves as the coincidence detector, then upon pairing with dopamine input (US), the cAMP levels in the odor-evoked Kenyon cells (CS+) should be notably elevated in comparison to the remaining KCs. A recent report demonstrated that the axo-axonic connections mediated by the muscarinic type-B receptor exert a suppressive effect on dopamine-evoked cAMP in neighboring KCs, thereby preventing weakly activated and unreliably responding KCs (off-target KCs) from being erroneously classified as the genuine CS+ KCs. This phenomenon of lateral inhibition is deemed essential for

memory formation (Manoim et al., 2022). To the best of our knowledge, there is no direct evidence that the cAMP levels in CS+ KCs are higher than those in the remaining KCs following classical conditioning. However, this serves as a crucial indicator of AC functioning as the coincidence detector. Therefore, live imaging should ideally be conducted at a cellular resolution, with the CS and US provided by presenting odors and electric shocks, respectively, to replicate the parsimony of coding and the authenticity of signals. With this objective in mind, we established an imaging system that simultaneously records cAMP and calcium transients in the KCs of head-opened Drosophila melanogaster observed under a two-photon microscope. We verified that odor presentation (CS) evoked not only calcium influx but also dopamine release (Mao and Davis, 2009; Riemensperger et al., 2005) and discovered that it induced robust cAMP increases even in the absence of the US, in axons that did not exhibit elevated calcium levels. This substantial cAMP elevation, which is dependent on dopamine signaling but not on calcium concentration, raises questions about the long-established fundamental understanding of conditioning mechanisms. Based on re-evaluations of the CS- or US-evoked cAMP, calcium, and dopamine transients, PKA activity, and acetylcholine (ACh) release in KCs at near single-cell resolution, we discuss what has been overlooked in the Drosophila model of classical conditioning.

Results

Odor presentation evokes cAMP elevation in a broad population of KCs independently of calcium responses

The mushroom bodies (MBs) in the Drosophila brain are the locus of olfactory classical conditioning (Heisenberg, 2003). The ~2,000 Kenyon cells (KCs) of the MBs are classified into three subtypes that extend axons into the α/β, α'/β', and γ lobes (Crittenden et al., 1998)(Figure 1A). These lobes can be subdivided anatomically and functionally into 15 non-overlapping compartments, each innervated by distinct dopamine neuron (DAN) populations (Aso et al., 2014; Tanaka et al., 2008). In Drosophila olfactory conditioning, Rutabaga adenylyl cyclase (Rut AC) is thought to serve as the coincidence detector in KCs (McGuire et al., 2003; Zars et al., 2000)(Figure 1B). Dubnau and his colleagues have shown that Rutabaga adenylyl cyclase expression is required in both α/β KCs and γ KCs to support aversive memory fully (Blum et al., 2009), while the dopamine receptor Dop1R1 expression in γ KCs is sufficient to support aversive memory (Qin et al., 2012). In addition, protocerebral posterior lateral 1 (PPL1) cluster dopamine neurons (DANs) projecting to the γ1, γ2, and α3 compartments and protocerebral anterior medial (PAM) cluster DANs projecting

122 to the γ3 compartment of KCs reinforced negative valence (Aso et al., 2012; Yamagata
123 et al., 2016). Elevations of cAMP levels and protein kinase A (PKA) activity reportedly
124 exhibited a synergistic effect following the pairing of a conditioned stimulus and an
125 unconditioned stimulus in the α lobe in the context of aversive conditioning paradigms
126 (Gervasi et al., 2010; Tomchik and Davis, 2009), and in the γ lobe in the context of
127 appetitive conditioning paradigms (Handler et al., 2019). Thus, we focused on the γ
128 and α lobes in subsequent live imaging experiments. Responses to odors were
129 measured as calcium transients with the genetically encoded fluorescent sensor
130 jRGECO1b (Dana et al., 2016) and cAMP levels were measured with G-Flamp1 (Wang
131 et al., 2022) simultaneously.

132 The two sensors were initially expressed with the γCRE-p GAL4 driver
133 (Yamazaki et al., 2018), as it encompasses a smaller subset of γ KCs compared to
134 other γ KC drivers, enabling the ability to achieve single-cell resolution within a dense
135 neuropil. Specifically, the γCRE-p driver covers approximately 350 (Yamazaki et al.,
136 2018) out of 701 γ KCs (Li et al., 2020). The γ lobe comprises five compartments, with
137 the γ1 compartment being the most distal. Initially, imaging of the γ2-5 compartments
138 was performed to achieve the optimal balance of resolution and scanning speed
139 (Figure 1C). In general, a sequence of images, with a consistent focus, was captured

140 at a frequency of approximately 2 frames per second, while three distinct olfactory
141 stimuli, specifically 3-octanol (OCT), 4-methyl cyclohexanol (MCH), and apple cider
142 vinegar (ACV), each with a duration of 3 seconds, and an electrical shock lasting 10
143 milliseconds, were successively administered. Prominent calcium responses were
144 observed in a limited number of axons (Figure 1C), reflecting the sparse coding nature
145 of KCs (Honegger et al., 2011). The γ KC axons branch and traverse the lobe in a
146 meandering manner, as depicted schematically in Figure 1A, resulting in single-plane
147 images of calcium responses often appearing interrupted and patchy. As previously
148 reported (Wang et al., 2022), we also detected odor-evoked cAMP signals with the
149 second channel, which varied in a compartment-specific manner along the length of
150 the lobes with distinct characteristics for each odor, and the most robust signal was
151 identified within the γ4 compartment upon MCH or ACV presentation (Figure 1D).
152 Notably, there was no evidence of cAMP being selectively synthesized in odor-
153 responding (as marked by the calcium signals in Figure 1C) axons. A marked increase
154 in cAMP was temporally delayed relative to the rise in Ca^{2+} levels in a population of
155 axons spanning almost the entire width of compartments, although there were
156 variations in levels among individual compartments. Conversely, the calcium signal
157 was sparsely detected, indicative of a restricted number of Kenyon cells responding to

158 a specific odor. These profiles suggest that cAMP levels do not exhibit a proportional
159 relationship with calcium concentrations, but rather are regulated as a compartmental
160 unit. An electrical stimulus elicits cAMP synthesis in the γ2 compartment, albeit with
161 variable signal strength (Figure 1C). Thus, the fly's behavior should be vigilantly
162 monitored each time the electrical stimulus is administered, and the shock responses
163 must be confirmed. Note that only a minimal increase in calcium levels was detected
164 following electrical stimulation. Additionally, the split GAL4 driver MB364B, which is
165 expressed in α/β and γ KCs, was used to eliminate any potential bias in cAMP
166 signaling, as the γCRE-p driver consists of 12 tandem CRE (cAMP responsive
167 element) sequences in the control region (Yamazaki et al., 2018)and may be more
168 likely to drive a population of cells responsive to cAMP signaling. The γ1-5
169 compartments were similarly subjected to imaging upon exposure to comparable
170 olfactory and electrical stimuli. The calcium and cAMP transient profiles in MB364B-
171 positive γ KCs were virtually congruent with those observed in γCRE-p KCs (Figure
172 1E). A significant increase in cAMP levels was noted in axons traversing nearly the full
173 breadth of the γ lobe, whereas the calcium signal was only discernible in a limited
174 number of axons. An electrical stimulus elicited cAMP synthesis in the γ1 and γ2
175 compartments, and in γ3 to a lesser extent. Responses in β KCs were also imaged

176 using the MB364B driver; however, they were not further analyzed. We subsequently
177 used the OK107 driver to visualize the α3 compartment, which was similarly subjected
178 to olfactory stimuli and electrical stimulation. A transverse optical section of the densely
179 packed neuropil in the α3 compartment enabled the observation of all α KCs within a
180 single focal plane. This view unequivocally illustrated that cAMP synthesis is subject to
181 compartmental regulation, as indicated by the considerable increase in cAMP levels
182 observed in the majority, if not all, of KCs upon exposure to MCH or OCT, while
183 uniformly minimal responses were detected upon exposure to ACV, regardless of
184 individual KCs' odor-specific calcium responses (Figure 1F-H). In summary, the cAMP
185 levels display odor-specific and compartment-dependent patterns, regardless of
186 calcium levels. Our focus will be on investigating the behavior of γ KCs, as the γ1 and
187 γ2 compartments are the sites of short and mid-term aversive memory formation (Aso
188 et al., 2010; Aso and Rubin, 2016).

189 **Dopamine elicits cAMP synthesis**

190 We subsequently inquired whether the dopamine signal modulates the cAMP synthesis
191 elicited by odor stimulus, given that odor-evoked cAMP transients vary among odors
192 and odors activate DANs (Figure 1B) (Cervantes-Sandoval et al., 2017; Mao and
193 Davis, 2009; Riemensperger et al., 2005; Sun et al., 2020). The widespread

194 dissemination of cAMP within compartments may be attributed to dopamine's release
195 through the process of volume transmission (Liu et al., 2021). We subsequently
196 employed $GRAB_{DA}$ (Sun et al., 2020) and Pink Flamindo (Harada et al., 2017)
197 simultaneously in the γ lobe, to assess the geometric correlation between the
198 dopamine and cAMP signals, respectively. An example showed the interrelatedness
199 between the two signals: the elevation in cAMP levels was temporally delayed relative
200 to the rise in dopamine levels (Figure 2A, D and G). However, caution must be
201 exercised when drawing conclusions at the cellular level, given the divergent kinetics
202 between these two sensors and the comparatively lower signal-to-noise ratio of Pink
203 Flamindo compared to G-Flamp1. To further elucidate the role of dopamine, we
204 measured the cAMP levels in a functionally null mutant of the type I dopamine
205 receptor, Dop1R1 (Akiba et al., 2019), which is coupled with GαS (Sugamori et al.,
206 1995) and thus engaged in activating adenylyl cyclase. The cAMP signals showed
207 substantial attenuation in the Dop1R1 mutant, thereby implying the necessity of the
208 dopamine signal for the activation of adenylyl cyclase (Figure 2B, C, E and F). It is
209 worth noting that the simultaneously recorded calcium signal was significantly
210 augmented when odors were presented, in comparison to the genetic control (Figure
211 2H). These experiments showed that odor stimulus alone evokes cAMP synthesis by

212 activating both PPL1 DANs (Figure 1B), which project to the γ1 and γ2 compartments,
213 and PAM (protocerebral anterior medial) DANs, which project to the γ3-5
214 compartments. PPL1 DANs also reinforce electric shock and PAM DANs also reinforce
215 sugar reward, the US, implying that the presentation of the odors, CS, is inextricably
216 linked with the presentation of the US.
217

218 **The cAMP levels are not regulated by calcium levels when odor and electric**
219 **shock are paired**

220 As previously noted, the long-held principle of coincidence detection posits that cAMP
221 levels in CS+ KCs should be specifically elevated when the odor stimulus and electric
222 shock are paired. How does this occur, despite the fact that the odor-evoked cAMP rise
223 does not depend on the calcium concentration, but on dopamine released from the
224 same PPL1 neurons that also reinforce the shock information? To answer this
225 question, we conducted imaging of calcium and cAMP transients in the γ lobe of head-
226 fixed flies that expressed G-Flamp1 and jRGECO1b driven by the γCRE-p or 364B
227 GAL4 driver and were subjected to OCT in conjunction with the administration of
228 electric shock, replicating the established paradigm of aversive memory conditioning.
229 Electric shock increased cAMP levels in the γ1-2 compartments (Figure 1E), as two

230 sets of PPL1 DANs, γ1pedc and γ2α'1, are known to convey aversive signals. We
231 examined the cAMP transients specifically in the γ1 and γ2 compartments in an
232 enlarged imaging field. A substantial augmentation in cAMP was noted throughout the
233 entirety of each compartment, independent of the localized increase in calcium levels
234 (Figure 3A). In the γ1 compartment of the fly harboring the γCRE-p GAL4 driver, the
235 degree of elevation in response to the simultaneous application of OCT and shock was
236 nearly equivalent to the summation of responses to each stimulus presented
237 independently (Figure 3B). However, in the γ2 compartment, the degree of elevation
238 was even lower than the sum of the responses to each stimulus applied independently
239 (Figure 3B). These results were not unexpected, as the cAMP levels rely largely on the
240 dopamine release facilitated by the same DANs activated by both CS and US.
241 However, these findings are in stark contrast to previous reports that a synergistic
242 increase; i.e., larger than a simple sum, of cAMP or PKA levels was observed upon
243 association of the two stimuli (Gervasi et al., 2010; Tomchik and Davis, 2009).

244 The correlation between calcium and cAMP levels was further evaluated using
245 scatterplots (Figure 3C). We examined representative images. No significant
246 associations were observed between calcium and cAMP levels (γ1: R^2 = 0.0076, γ2: R^2
247 = 0.0881). It is worth contemplating that roughly 5% of KCs manifest temporal

248 dynamics that give rise to an elevation in calcium levels (Honegger et al., 2011), while
249 a significant majority of KCs synthesize cAMP in response to dopaminergic stimulation
250 upon exposure to a particular olfactory stimulus. Hence, it is plausible for the calcium
251 and cAMP signals to exhibit some degree of overlap, even in the absence of a
252 causative link between the two signals. On the contrary, assuming the complete
253 dependency of cAMP synthesis on calcium levels, the plot could be simulated in the
254 following manner. The timeline images extracted from the identical bout of calcium
255 imaging employed in Figure 3C were segregated into odd-numbered and even-
256 numbered images, and subjected to a scatterplot analysis against each other, thereby
257 simulating the representation of calcium levels in even-numbered frames as cAMP
258 levels (Figure 3D). This simulation yielded R^2 values of 0.462 (γ1) and 0.756 (γ2).

259 Thus, while we cannot dismiss the possibility that cAMP synthesis may require a
260 specific threshold of calcium, it is irrefutable that the cAMP levels are not entirely
261 contingent upon calcium levels even when odor and electric shock are paired. In other
262 words, the concentration of cAMP alone does not serve as a cellular engram that
263 distinguishes the KCs that respond to the CS+ odor from the rest of the KCs.
264

The cAMP code of an odor is integrated with the cAMP code of an electric shock during conditioning

As described, the cAMP level in the γ1-2 compartments depends on dopamine transmitted by PPL1 DANs (Aso et al., 2012) and that in the γ3-5 compartments by PAM DANs (Liu et al., 2012; Yamagata et al., 2016). Moreover, discrete compartments can be identified in relation to odor valence, wherein DANs that innervate the γ2 compartment are indicative of an aversive olfactory valence, whereas those innervating the γ4 compartment are indicative of an appetitive olfactory valence (Kato et al., 2023; Siju et al., 2020) Furthermore, DANs integrate odor valence and shock signals (Huang et al., 2022). Given the hypothesis that cAMP acts as an intermediary for dopamine's role in determining odor valence, achieving a state of balanced cAMP levels across the γ lobe could provide a representation of integrated valence as part of the overall valence encoded within the entire KC compartments. This can be visualized as a two-dimensional image displaying cAMP levels across different compartments (Figure 2C) and is referred to as the cAMP code. We posited that the cAMP code might represent the neural plasticity mechanism engaged in aversive conditioning. Although the absolute cAMP levels exhibited variations among individuals for each odor, we hypothesized that the relative cAMP levels of the γ2 (corresponding to negative

283 valence) and γ4 (corresponding to positive valence) compartments, the γ2/4 cAMP
284 ratio, may constitute a quantitative metric for evaluating the valence of an olfactory
285 stimulus for an individual. As such, any variations in the γ2/4 cAMP ratio prior to and
286 post-conditioning could be employed to assess the differential response to the
287 stimulus, reflecting the acquisition of memory. To this end, we attempted to replicate
288 aversive conditioning by subjecting the fly to three consecutive episodes of electric
289 shocks while exposing it to OCT, followed by exposure to MCH and ACV without
290 electric shocks (OCT as CS+), or exposing it to MCH with electric shocks and to OCT
291 and ACV without electric shocks (MCH as CS+), while observing it under a microscope
292 (Figure 4A). During the process, cAMP transients were recorded for each exposure
293 and quantified. Averaged images of a single sample and profiles of cAMP transients
294 from pooled samples are presented (Figure 4B and E). Note that, based on the innate
295 behavioral responses, OCT and MCH are both similarly aversive compared to air,
296 whereas ACV is attractive (Badel et al., 2016). The administration of electric shock
297 resulted in heightened cAMP levels within the γ1-3 compartments. In this and
298 subsequent quantifications, the signal emanating from the γ1 compartment was
299 excluded from statistical analyses due to the divergence in the focal plane utilized for
300 γ1 signal detection compared to other compartments. Consequently, not all brain

301 samples included data from the γ1 compartment. During the conditioning protocol
302 where OCT was paired with electrical shock, there was an increase in cAMP within the
303 γ2 compartment, as described (Figure 3), but these modifications did not attain
304 statistical significance in the series of experiments described here (Figure 4B, E and
305 K). This was in parallel with a significant decrease of cAMP levels in the γ4
306 compartment. Subsequent to the associative conditioning, the presentation of OCT
307 reverted cAMP levels to pre-conditioning states in the γ2 compartment, while
308 maintaining lower cAMP levels in the γ4 and γ5 compartments relative to pre-
309 conditioning states (Figure 4H), thereby preserving an elevated γ2/γ4 cAMP ratio post-
310 conditioning. No significant changes in the g2/4 cAMP ratio were detected in MCH or
311 ACV, which were not conditioned with an electric shock (Figure 4N). Conversely, when
312 MCH was conditioned with an electric shock, there was an increase in the γ2/4 cAMP
313 ratio of MCH, albeit to a lesser degree, while no significant alteration was observed in
314 either OCT or ACV (Figure 4C, F, I, L and O).
315 We next conducted the conditioning experiment with flies, wherein PPL1
316 DANs were specifically ablated through the expression of the tetanus toxin (TNT) light
317 chain (Sweeney et al., 1995), utilizing the TH-LexA > LexAop-TNT system
318 (Karuppudurai et al., 2014)(Figure 4D, G, J, M and P). DANs located within the PPL1

cluster are known for transmitting aversive information to the γ1 and γ2 compartments. Despite this targeted ablation, weak cAMP signals persisted in the γ1 and γ2 compartments upon odor presentation but not upon shock delivery (Figure 4Q-R), possibly due to the influence of other signals. Note that the peak of these cAMP responses was delayed by two seconds compared to the control (Figure 4S) and was absent during shock administration. We did not observe neural plasticity associated with conditioning, and specifically no alterations in the γ2/4 cAMP ratio (Figure 4P), thereby reaffirming the significant role of PPL1 DANs in the context of aversive conditioning. Interestingly, in the γ 3-5 compartments of PPL1 dopamine neuron-ablated flies, the levels of cAMP were elevated compared to the control group. Considering the projection of PAM class dopamine neurons into the γ 3-5 compartments, this finding again suggests a reciprocal regulatory mechanism between PPL1 DANs and PAM DANs. This implies the existence of a circuit mechanism that regulates activities across PPL1 and PAM dopaminergic neurons. This regulatory mechanism likely includes interneurons such as CRE011, which integrates inputs from 9 types of MBONs including γ2α’1 and provides inputs to reward DANs including γ4 (Shuai et al., 2024a).

Associative conditioning induces changes in dopamine levels, which subsequently result in alterations in the cAMP code

Given that the cAMP code is structured by the dopaminergic system, we inferred that cAMP dynamics would closely parallel those of dopamine during aversive conditioning. Flies containing both the $GRAB_{DA}$ and Pink Flamindo sensors, driven by the CRE-p GAL4 driver, but not by the 364B driver due to its effects on aberrant development, were subjected to aversive conditioning and observed under the microscope. Averaged images and time courses of ΔF/F0 for cAMP and dopamine levels are presented (Figure 5A - B). Both signals exhibited a strong correlation, even throughout the conditioning process, with dopamine levels rising earlier and more abruptly than the increase in cAMP (Figure 5A - C'). It is important to note that the dopamine levels in the γ2 compartment observed during the conditioning process surpassed those observed when either the olfactory stimulus or electrical shock was administered alone, although these modifications did not attain statistical significance (Figure 5C and D). Conversely, a significant reduction in dopamine levels was observed in the γ4 compartment (Figure 5C and D). These alterations were reflected in the concurrently recorded cAMP levels (Figure 5C' and D'). This suggests that the changes in cAMP levels during conditioning can be attributed to the changes in dopamine levels, rather than a synergistic

355 interaction between dopamine and calcium acting upon the Rutabaga adenylyl cyclase.
356 Following conditioning, the dopamine γ2/4 ratio, upon exposure to the conditioned
357 stimulus paired with OCT (CS+OCT), became markedly elevated compared to the ratio
358 observed prior to conditioning. This increase parallels the changes noted in the cAMP
359 γ2/4 ratio (Figure 5 E and E').
360

361 **The protein kinase A (PKA) activities coincide with the presence of cAMP**

362 Protein kinase A (PKA) is a prominent subject of cAMP modulation, making it a suitable
363 indicator to probe the functional status of the observed cAMP population. We employed
364 the expression of a PKA sensor, ExRai-AKAR2 (Zhang et al., 2021), in combination
365 with Pink Flamindo, to examine whether the PKA activity aligns with the spatial
366 distribution of cAMP. The temporal extent of the alterations in PKA activities exhibited a
367 more prolonged persistence compared to that of cAMP (Figure 6B). Despite the
368 constraints posed by the signal-to-noise ratios of these sensors, which impeded our
369 comprehensive examination of signals at a cellular level, the dynamics of PKA
370 activities unveiled a profound correlation with the cAMP signal (Figure 6A). This
371 correlation was not only apparent within individual compartments but also manifested
372 as a population code, mirroring the cAMP code throughout the entirety of the memory

373 acquisition process (Figure 6A-C).

374

375 **The role of the Rutabaga adenylyl cyclase**

376 The Rutabaga adenylyl cyclase has been regarded as the coincidence detector, as

377 described, and indeed demonstrated to increase cAMP levels synergistically only in the

378 presence of both the CS and US (Gervasi et al., 2010; Tomchik and Davis, 2009). We

379 failed to observe the anticipated synergistic elevation of cAMP levels upon pairing CS

380 and US in the fly harboring wild-type Rutabaga, and only observed additive elevation

381 (Figure 3B). Nevertheless, we were still contemplating what we might observe in the *rut*

382 mutants, given the pivotal role of rut in aversive memory formation.

383 *rutabaga*^{1} (*rut*^{1}), which is well known for its distinctive learning deficit phenotype

384 in the context of aversive memory, was initially isolated from the X chromosome

385 collection mutagenized by ethyl-methanesulfonate (Livingstone et al., 1984). This

386 mutation bears a point mutation that leads to the total loss of its adenylyl cyclase

387 activity (Levin et al., 1992). We assessed cAMP transients using G-Flamp1 in the *rut*^{1}

388 flies during aversive conditioning, adhering to the aforementioned experimental

389 protocol, with OCT serving as the conditioned stimulus (Figure 7B, D, F, H and J). The

390 cAMP levels in the *rut*^{1} flies were not significantly lower compared to the control group

391 (Figure 7A-F), implying that Rutabaga's contribution to cAMP production in the KCs is
392 limited as previously reported (Noyes and Davis, 2023; Tomchik and Davis, 2009).
393 Nonetheless, we subsequently detected distinct cAMP codes in the *rut*^{1} flies compared
394 to the control flies, even prior to the conditioning phase. In the *rut*^{1} mutant, when
395 aggregating all instances of odor exposure (MCH, OCT, and ACV), cAMP levels were
396 higher in the γ2 compartment and lower in the γ4 compartment as compared to the
397 genetic control (Figure 7K). In response to shock, cAMP levels in the γ4 compartment
398 were elevated in the *rut*^{1} mutant relative to the genetic control, while those in the γ2
399 compartment remained comparable (Figure 7L). During the conditioning procedure, the
400 cAMP increase in the γ2 compartment or the decrease in the γ4 and γ5 compartments
401 in the *rut*^{1} mutant was less pronounced than that in the control group (Figure 7G-H).
402 These phenomena led to a γ2/4 ratio that remained unchanged after the conditioning
403 process (Figure 7 I, J), consistent with the impaired aversive memory formation linked
404 to *rut*^{1}.

405

406 **cAMP depresses ACh release from KCs**

407 The KCs are recognized as cholinergic (Barnstedt et al., 2016; Yasuyama and
408 Salvaterra, 1999), and their ACh release after aversive conditioning is reportedly

409 attenuated in the γ1 (Zeng et al., 2023)γ2 and γ3 (Stahl et al., 2022; Zeng et al.,
410 2023)and α3' compartments (Zhang et al., 2019). It was recently reported that
411 Rutabaga decreases ACh release from KCs upon conditioning (Noyes and Davis,
412 2023). Our findings were in concordance with these observations. We conducted
413 simultaneous imaging of ACh and cAMP transients in the γ KCs of flies expressing the
414 ACh sensor, $GRAB_{ACh\ 3.0}$, and Pink Flamindo, under the control of the MB364B GAL4
415 driver. Subsequently, aversive conditioning was administered to the flies while they
416 were observed under the microscope (Figure 8). In the genetic control group, in
417 response to exposure to the CS+ OCT odor, there was a significant reduction in
418 relative cAMP levels within the γ4 and γ5 compartments following electric shock
419 conditioning (Figure 8 A, D and G), as previously described. ACh levels decreased
420 within the γ1 and γ2 compartments but remained constant within the γ4 and γ5
421 compartments (Figure 8 A', D' and G'), leading to a decrease in the γ2/4 ACh ratio and
422 an elevation in the γ2/4 cAMP ratio following conditioning (Figure 8 J). No such
423 changes were observed in CS- MCH or ACV. This becomes apparent when the
424 responses in cAMP and ACh are simultaneously visualized in a two-dimensional plot
425 (Figure 8M). The relative levels of ACh do not consistently demonstrate a direct inverse
426 correlation with the levels of cAMP. This inverse correlation becomes notably

427 conspicuous in the response to the CS+ odor after conditioning (Figure 8M).

428 We conducted simultaneous imaging of ACh and cAMP transients in the *rut*[1]

429 background (Figure 8B, B', E, E', H, H', K and N). In this background, no significant

430 alterations in ACh transients were detected in either the γ2 or γ4 compartment, both

431 during and after the conditioning process (Figure 8 B', E' and H'). The response

432 trajectories of cAMP and ACh release in the *rut*[1] mutant displayed notable uniformity

433 across diverse olfactory stimuli, regardless of the conditioning status (Figure 8N). This

434 contrasts with the diverse response patterns observed in the genetic control (Figure

435 8M). The levels of ACh release in the γ2 and γ4 compartments were higher compared

436 to the genetic background, irrespective of their cAMP levels (Figure 8P). These

437 observations suggest that the Rut adenylyl cyclase plays an indispensable role in the

438 modulation of synaptic plasticity.

439 We subsequently analyzed the ACh responses following exposure to three

440 distinct olfactory stimuli in the Dop1R1 mutant, to examine if the steady state levels of

441 ACh are regulated by the dopamine signal (Figure 8C', F' and I'). In this context, we

442 observed a significant elevation in ACh levels compared to the genetic control (Figure

443 8Q). This finding contradicts previous reports indicating a reduction in ACh levels under

444 Dop1R1 knockdown conditions (Noyes and Davis, 2023) and aligns with the

445 hypothesis that ACh levels are decreased by dopamine and/or cAMP.

446 Subsequently, we proceeded to monitor the release of ACh by activating
447 adenylyl cyclase through the bath application of Forskolin, aiming to investigate
448 whether cAMP, rather than another component downstream of dopamine, attenuates
449 the ACh release (Figure 9). Upon Forskolin administration, we observed a remarkable
450 increase in the cAMP levels, concurrent with a reduction in the ACh levels, in the γ2
451 compartment (Figure 9A and B). The Forskolin administration also reduced ACh
452 release in response to odor (OCT) presentation, with subsequent recovery following
453 Forskolin washout (Figure 9C and D).

454

455

456 **Discussion**

457 Our study demonstrates that cAMP levels do not differentiate CS+ KCs from the
458 remaining KC population. Instead, cAMP acts as a reinforcer downstream of dopamine,
459 suppressing acetylcholine release from KCs and consequently modulating the DAN-
460 KC-MBON recurrent feedback loop (Adel and Griffith, 2021; Cognigni et al., 2018;
461 Felsenberg et al., 2018, 2017; Jovanoski et al., 2023; Kato et al., 2023; Li et al., 2020;
462 Modi et al., 2020; Otto et al., 2020; Rubin and Aso, 2023) in a valence-dependent

463 manner. We hereby propose that the cAMP levels across the γ compartments of the
464 mushroom body can be designated as the "cAMP code", which serves as an indicator
465 of the integrated valence experienced by the individual. In this context, we posit that
466 the cAMP code can holistically encode a memory engram.

467

468 **The levels of cAMP do not differentiate CS+ KCs from other KCs**

469 Physiological and cellular studies on Aplysia gill withdrawal (Abrams and Kandel, 1988;
470 Ocorr et al., 1985; Yovell et al., 1992) and genetic studies on Drosophila olfactory
471 conditioning (Heisenberg, 2003; Levin et al., 1992; Livingstone et al., 1984; Mons et al.,
472 1999; Tully, 1987; Tully and Quinn, 1985) solidified the idea of adenylyl cyclase as a
473 coincidence detector. This also holds for vertebrates. For example, pre-post pairing
474 (CS) and dopamine (US) signals are thought to converge on adenylyl cyclase in reward
475 learning (reward prediction error) in the striatum (Urakubo et al., 2020; Yagishita et al.,
476 2014).

477 Our research aimed to directly examine this long-standing hypothesis by
478 observing the *in vivo* cAMP and calcium or dopamine transients at near single-cell
479 resolution, which revealed some incongruities. First, the presentation of an odor elicits
480 dopamine release from the same populations of DANs that mediate shock signals, as

481 previously reported (Mao and Davis, 2009; Riemensperger et al., 2005), demonstrating
482 that the CS is invariably coupled with the US. Indeed, the odor presentation alone
483 induces a robust elevation of cAMP levels in KCs, independent of their response to the
484 relevant odor. The anticipated synergy was not detected, as we failed to observe a
485 specific increase in cAMP levels in CS+ KCs, even in the γ1 and γ2 compartments,
486 which are indispensable and adequate for the acquisition of short- and middle-term
487 memories (Aso et al., 2012). These results contradict the notion that the concentration
488 of cAMP alone serves as the cellular engram for association (Figure 10A). In
489 considering this variability, we cannot definitively exclude the possibility that the
490 electrical stimulation was suboptimally delivered. Our method entailed the deployment
491 of three consecutive 60-volt electrical shocks, each with a tenure of 10 milliseconds.
492 Verification of this protocol came from observations of the flies' leg flailing and brief
493 abdominal spasms—responses that signify effective shock delivery. Nonetheless, the
494 flies manifested olfactory-triggered responses, confirmed by calcium imaging and the
495 initiation of ambulatory leg motions, the sporadic activity observed in response to
496 olfactory stimuli, signifying maintained physiological integrity. However, upon increasing
497 the shock duration to 20 milliseconds, while calcium imaging continued to reflect
498 olfactory responses, there was an absence of autonomous leg activity following the

499 administration of two consecutive shocks. It should be noted that following the
500 conditioning procedure employed in this study, we observed a significant reduction in
501 Ach release within the γ2 compartment, a phenomenon recognized as the engram of
502 aversive memory (Noyes and Davis, 2023; Stahl et al., 2022). These insights imply that
503 the experimental parameters we employed were both necessary and adequately
504 calibrated.

505 An additional consideration is that we cannot formally preclude the possibility
506 that the core site of the Rutabaga action or the coincidence detection was within a
507 microenvironment that we failed to access, or the population of cAMP synthesized with
508 Rutabaga at the coincidence detection was masked by the pool of cAMP synthesized
509 with other adenylyl cyclases. The overlap between the positive PKA and cAMP signals
510 suggests that the cAMP signal detected in the current study was sufficiently functional
511 to activate PKA. The following discussion is based on the assumption that the detected
512 cAMP signal is functional. Although our findings indicate that the CS+ KCs cannot be
513 differentiated from the other KCs based on cAMP levels, the cAMP signal still holds
514 significant importance in memory formation. In the realm of mammalian reward
515 learning, the convergence of calcium-mediated NMDAR signaling and dopamine has
516 been demonstrated and modeled to occur on AC (Urakubo et al., 2020; Yagishita et al.,

517 2014). Nair et al. presented a theoretical framework wherein the cAMP/PKA signal
518 activated by dopamine converges with the calcium signal at CaMKII, when the inputs of
519 calcium and dopamine are delivered in temporal proximity and in a dopamine-
520 following-calcium sequence (Nair et al., 2016). This role of CaMKII could underlie the
521 case of Drosophila olfactory conditioning, since CaMKII accumulation in the KC axons
522 is required for Drosophila aversive and appetitive conditioning (Adel et al., 2022; Chen
523 et al., 2022; bur see also Yamada et al., 2024).
524 The Rutabaga AC is not necessarily involved in all phases of aversive
525 olfactory memory, as it is crucial for labile anesthesia-sensitive memory (ASM), but
526 dispensable for anesthesia-resistant memory (ARM). In contrast, the Dunce
527 phosphodiesterase 4 is essential for ARM, but not for ASM, despite both Rutabaga and
528 Dunce serving in the cAMP pathway (Scheunemann et al., 2012). Additionally, the
529 presence of Rutabaga is concurrently required within both α/β and γ KCs, whereas
530 Dunce operates in both KCs and antennal lobe local neurons (Scheunemann et al.,
531 2012). Another olfactory memory paradigm, known as "trace conditioning," does not
532 require the Rutabaga AC and allows the presentation of the conditioned stimulus (CS)
533 and the unconditioned stimulus (US) to be temporally separated by intervals of up to 60
534 s (Shuai et al., 2011). The Rutabaga AC has been identified as the sole type-I AC in

535 Drosophila (Livingstone, 1985), and its activation by calcium and the GαS subunit has
536 led to its postulation as a coincidence detector for the CS and US. This implies that the
537 underlying mechanism for the convergence of ARM and trace conditioning relies on
538 another AC or an alternative mechanism.
539
540 **Another model for coincidence detection**
541 Several research findings have revealed an alternative mechanism of coincidence.
542 Saitoe et al. showed that the aversive input of electric shocks is conveyed by
543 glutamate, but not dopamine; rather, dopamine release is elicited after this pairing
544 event and serves solely as a reinforcement, but not the US (Saitoe, 2021; Ueno et al.,
545 2017). They further demonstrated that the glutamate transmission is mediated by the
546 ensheathing glia (EG) that surround the MBs (Miyashita et al., 2023). Yamada and
547 Hige recently demonstrated that the targeted application of forskolin alone does not
548 induce presynaptic plasticity (Yamada et al., 2024), manifested as long-term
549 depression (LTD), which is characteristically observed at the KC-MBON synapse after
550 the associative pairing of olfactory cues with aversive stimuli (Hige et al., 2015).
551 However, when the optogenetic stimulation of Kenyon cells is coupled with the
552 application of forskolin, LTD is indeed induced, implying that these two inputs converge

553 somewhere downstream of cAMP synthesis (Yamada et al., 2024). Qiao et al.
554 demonstrated that the PPL1 DANs modulate the input-timing-dependent plasticity of γ
555 KC synapses from projection neurons, depending on type 2 dopamine receptor (DD2R)
556 (Qiao et al., 2022). Their findings further indicated that the activation of the PPL1-
557 DD2R pathway elicits a rise in calcium levels, which is dependent on the voltage-gated
558 calcium channel (VGCC). They concluded that the VGCC could serve as the
559 coincidence detector. However, this conclusion does not extend to all phases of
560 aversive memory, as the authors also demonstrated that DD2R is not necessary for
561 short-term memory formation.
562 The potential role of the DAN-KC-MBON recurrent feedback loop in the
563 formation of olfactory memory raises the prospect that the synaptic connections
564 between KCs and MBONs may also rely on spike-timing-dependent plasticity (STDP)
565 (Zeng et al., 2023). Between KCs and MBONs in locusts, Cassenaer and Laurent have
566 shown that pre-post pairing causing STDP can, when accompanied by the local
567 administration of a reinforcement-modulating neuromodulator such as dopamine
568 (three-factor neo-Hebbian learning rule), designate the synapses subject to an
569 associative alteration (Cassenaer and Laurent, 2012). This is likely to apply to
570 Drosophila as well. It is noteworthy that comprehensive anatomical studies have

disclosed direct dopaminergic connections from DANs to MBONs in Drosophila α/β KCs (Takemura et al., 2017). Pribbenow et al. have indeed demonstrated that concurrent dopamine release and focal acetylcholine application to M6 (MBON-γ5β'2a) dendrites, circumventing KC activity, induce plasticity in calcium transients within this MBON (Pribbenow et al., 2022). Zeng et al. further found that the dorsal paired medial (DPM) neuron releases 5-HT on KCs and regulates the coincidence time window, which has been hypothesized by several theories to be a timing regulator (Zeng et al., 2023).

The dopamine population activities serve as the substrate for the storage of aversive olfactory memory

Upon exposure to different odors, distinct populations of DANs exhibit specific activity patterns, as documented in multiple studies (Berry et al., 2012; Huang et al., 2022; Kato et al., 2023; Mao and Davis, 2009; Yamagata et al., 2016). This, in turn, generates the cAMP code in the γ lobe, which is approximately antithetical to the level of ACh release (Figure 10B). Given that the sustained population dynamics among DANs, likely facilitated by the dynamic interactions within the DAN-KC-MBON recurrent feedback loop, integrate changes in physiological states and environmental cues

589 (Huang et al., 2022; Kato et al., 2023; Siju et al., 2020), the formation of associative
590 memories could be an integral component of this dynamism. This is consistent with the
591 additional finding that repeated exposure to an aversive odor can give rise to a labile,
592 self-reinforced aversive memory for that odor (Jacob et al., 2021). If the odor and
593 electric shock stimuli are expressed as the cAMP code, then it can be posited that the
594 electric shock serves as an extreme manifestation of the odor stimuli, since both
595 olfactory stimuli (CS) and electric shock (US) activate overlapping populations of
596 DANs. The imaging of dopamine levels indeed confirms this assertion. The alterations
597 in dopamine levels observed during the conditioning process were reflected in the
598 concurrently recorded cAMP levels, suggesting that the integration of the CS and US
599 takes place at the dopamine level (Figure 10C). Thus, in this particular memory
600 paradigm, there appears to be no significant distinction between the odor CS and the
601 electric shock US in terms of dopaminergic signaling. Assuming this to be true, the
602 inquiry into the location and mechanism of memorization for the learned population
603 activities of DANs could be comparable to the question of where and how odor-specific
604 population activities of DANs, in general, are retained.
605 In addition to the well-established function of the exogenously activated γ1-
606 pedc DAN as the aversive US (Aso et al., 2012; Aso and Rubin, 2016), the suppression

607 of the corresponding MBON, γ1-pedc>α/β, can also serve as an aversive US (König et
608 al., 2019; Ueoka et al., 2017), as noted (Yamada et al., 2023). These discoveries
609 suggest that not only the stimulation of the γ1pedc DAN, but also the inhibition of
610 γ1pedc>α/β MBON can trigger a series of events that tilt the population activities of
611 DANs towards the aversively learned state. Assuming that the population activities of
612 DANs are consistently revised by the DAN-KC-MBON recurrent feedback loop that
613 integrates inputs from relevant compartments, alterations in the γ1 compartment
614 triggered by augmented γ1 DAN activity or decreased γ1 MBON activity could
615 potentially trigger a complete rewrite of the population activities of DANs.
616 Recently, the postsynaptic plasticity traces associated with nicotinic
617 acetylcholine receptors in MBONs were reported to contribute to memory storage in
618 appetitive memory (Pribbenow et al., 2022), although their involvement in aversive
619 memory is yet to be established. The underlying cause of this plasticity can be
620 attributed to the previously described neo-Hebbian learning rule. However, it remains
621 unclear how this plasticity leads to changes in the population activities of DANs,
622 resulting in alterations in the shape of the cAMP code. Based on these assumptions,
623 we propose the following model for the formation of aversive olfactory memories. Upon
624 exposure to odor A paired with an electric shock, the release of ACh from the γ1 and

625 γ2 compartments of responsive KCs is attenuated because of the increase in cAMP
626 levels, leading to a depression of the γ1 and γ2 MBONs. This subsequently triggers the
627 reorganization of the dopamine population activities, as well as that of the ACh
628 receptors within the γ1 and γ2 MBON synapses. Consequently, the cAMP code for
629 odor A is shifted towards a more negative valence in comparison to its pre-conditioning
630 state. The cAMP pathway including PKA exerts inhibitory control over ACh release in
631 accordance with the population activities of DANs (Figure 10B). Despite the current
632 lack of knowledge regarding the higher-order mechanisms responsible for the
633 organization of the DAN-KC-MBON recurrent feedback loop, recent progress in
634 unraveling the hierarchical architecture of the DAN circuit (Rubin and Aso, 2024; Shuai
635 et al., 2024b; Yamada et al., 2023) holds promise for illuminating these mechanisms in
636 the near future.
637
638 **The role of Rutabaga AC**

639 The *rut*^{1} mutation was demonstrated to completely abolish Rutabaga AC activity (Levin
640 et al., 1992). However, in the *rut*^{1} mutant, cAMP levels were found to be either
641 comparable to or slightly lower than those in the control strain. This finding suggests
642 that substantial cAMP levels in KCs are maintained by alternative adenylyl cyclases. It

643 has indeed been shown that innate odor preferences are reliant on another adenylyl
644 cyclase, ACXD (Noyes and Davis, 2023). Nonetheless, short-term aversive memory is
645 impaired in the *rut*^{1} mutant, and this deficit can be ameliorated by expressing the wild-
646 type Rutabaga in γ and αβKCs (McGuire et al., 2003; Zars et al., 2000). This
647 underscores the crucial role of Rutabaga in the formation of aversive memory within γ
648 and αβKCs.

649 In our current imaging analyses of γKCs, we have made three significant
650 observations pertaining to the cAMP code specific to the *rut*^{1} mutation:
651 (1) The cAMP code in the *rut*^{1} mutant differs from that of the genetic control even prior
652 to conditioning, contrary to previous findings (Noyes and Davis, 2023). Specifically,
653 in the *rut*^{1} mutant, the relative cAMP level in the γ2 compartment is higher, whereas
654 the relative level in the γ4 compartment is lower. This suggests that the *rut*^{1} mutant
655 perceives these odors with a more negative valence than the wild type even before
656 conditioning.
657 (2) During conditioning, the cAMP levels in the γ2 and γ4 compartments remained
658 unchanged in the *rut*^{1} mutant, in contrast to the genetic control. This phenomenon
659 could be partly attributed to lower levels of cAMP in the γ2 compartment and
660 slightly higher levels in the γ4 compartment induced by electric shock in the *rut*^{1}

661 mutant, compared to the genetic control.

662 (3) cAMP potentially suppresses ACh release, a phenomenon particularly evident after

663 conditioning, where ACh levels across the γ lobe exhibit an inverse correlation with

664 the cAMP code (Figure 8M). However, in the *rut*^{1} mutant, ACh levels remain

665 unchanged post-conditioning and do not display an inverse correlation with the

666 cAMP code. In addition, compared to the genetic background, ACh levels in the

667 *rut1* mutant are higher, despite the fact that the cAMP levels in *rut*^{1} are not

668 significantly lower. This suggests that the inhibition of acetylcholine release may not

669 be a straightforward consequence of cAMP action and may involve Rutabaga-

670 specific adenylyl cyclase activity, as described (Noyes and Davis, 2023).

671 These characteristics provide an explanation for the impaired aversive

672 memory in the *rut*^{1} mutant. Among the family of adenylyl cyclases, the molecular

673 determinants that endow Rutabaga with its specialized role in mediating synaptic

674 plasticity have yet to be elucidated. This prompts the question of whether the specificity

675 of Rutabaga is attributable to its sensitivity to calcium ions, a hypothesis that has not

676 yet been substantiated through our research. To elucidate these points, further

677 physiological and biochemical studies will be necessary. Considering that the locus for

678 coincidence detection was established by rescuing the *rut*^{1} mutation, it may be

679 necessary to reevaluate this if Rutabaga does not contribute to this process.

680

681 **Materials and methods**

682 **Fly strains**

683 Fly strains were maintained on standard food containing cornmeal at 25°C. The
684 following strains were used. CRE-p65-AD/CyO; MB247-GAL4-DBD (Yamazaki, 2018),
685 UAS-G-Flamp1 attp40/CyO and UAS-G-Flamp1 VK00005 (gifts from Jun Chu and
686 Yulong Li, Nat. Commun., 2022.13:5363), TH-lexA vk00040 (a gift from Yoshinori Aso),
687 UAS-jRGECO1b VK00005 (#BL63795), MB364B-GAL4 i.e., R13F02-p65-AD attp40;
688 R21B06-GAL4-DBD attP2 (#BL68318), OK107-GAL4 (#Kyoto DGRC 106098), UAS-
689 Pink Flamindo su(Hw) attP5 and UAS-Pink Flamindo VK00027 (this study), UAS-
690 GRAB_DA2m attp40 (BL#90878), Dop1R1^{KO} (D1R1 KO, a gift from Taro Ueno, Eur. J.
691 Neurosci. 2020;51:822–839), UAS-ExRai-AKAR2 VK00005 (this study), and UAS-
692 GRAB_ACh3.0 attp40 (BL#86549).

693

694 **Fly genotypes used by figures**

Figure	Genotype

1C, 1D	CRE-p65-AD, UAS-G-Flamp1 attp40 / UAS-G-Flamp1 attp40; MB247-GAL4-DBD, UAS-jRGECO1b VK00005 / UAS-jRGECO1b VK00005
1E	R13F02-p65ADZp attP40 / UAS-G-Flamp1 attp40; R21B06-ZpGdbd attP2, UAS-jRGECO1b VK00005 / +
1F, 1G, 1H	UAS-G-Flamp1 attp40 / +; UAS- jRGECO1b VK00005 / + ; OK107-GAL4 / +
2A, 2D, 2G	CRE-p65-AD, UAS-GRAB_DA2m attp40, UAS-Pink Flamindo su(Hw)attp5 / UAS-GRAB_DA2m attp40, UAS-Pink Flamindo su(Hw)attp5; MB247-GAL4-DBD, UAS-Pink Flamindo VK00027 / +
2B, 2E	same as 1C
2C, 2F	CRE-p65-AD, UAS-G-Flamp1 attp40 / UAS-G-Flamp1 attp40; MB247-GAL4-DBD, UAS-jRGECO1b VK00005, Dop1R1^{KO} / UAS-jRGECO1b VK00005, Dop1R1^{KO}
2H	Control: same as 2A; Dop1R1$^{KO/KO}$: same as 2C
3A	left: same as 1C; right: same as 1E
3B, 3C, 3D	same as 1C
4B, 4C, 4E, 4F, 4H, 4I, 4K, 4L, 4N, 4O	same as 1E
4D, 4G, 4J, 4M, 4P	R13F02-p65ADZp attP40 / UAS-G-Flamp1 attp40; R21B06-ZpGdbd attP2, UAS-jRGECO1b VK00005 / TH-lexA vk00040, LexAop-TNT
4Q, 4R, 4S	control: same as 1E; TH-lexA>TNT: same as 4D
5A, 5A', 5B, 5B', 5C, 5C', 5D, 5D', 5E, 5E'	same as 2A
6A, 6A', 6B, 6B', 6C, 6C'	R13F02-p65ADZp attP40 / UAS-Pink Flamindo su(Hw)attp5; R21B06-ZpGdbd attP2 / UAS-ExRai-AKAR2 VK00005

7A, 7C, 7E, 7G, 7I	R13F02-p65ADZp attP40 / + ; R21B06-ZpGdbd attP2, UAS-G-Flamp1 vk00005 / +
7B, 7D, 7F, 7H, 7J	rut^1/ rut^1; R13F02-p65ADZp attP40 / + ; R21B06-ZpGdbd attP2, UAS-G-Flamp1 vk00005 / +
7K, 7L	control: same as 7A; $rut^{1/1}$: same as 7B
8A, 8A', 8D, 8D', 8G, 8G', 8J, 8M	R13F02-p65ADZp attP40, UAS-Pink Flamindo su(Hw)attp5 / UAS-GRAB_ACh3.0 attp40; R21B06-ZpGdbd attP2 / +
8B, 8B', 8E, 8E', 8H, 8H', 8K, 8N	rut^1/ rut^1; R13F02-p65ADZp attP40 / UAS-GRAB_ACh3.0 attp40, UAS-Pink Flamindo su(Hw)attp5; R21B06-ZpGdbd attP2 / +
8C, 8C', 8F, 8F', 8I, 8I', 8L, 8O	R13F02-p65ADZp attP40 / UAS-GRAB_ACh3.0 attp40, UAS-Pink Flamindo su(Hw)attp5; R21B06-ZpGdbd attP2, $Dop1R1^{KO}$ / $Dop1R1^{KO}$
8P	control: same as 8A; $rut^{1/1}$: same as 8B
8Q	control: same as 8A; $Dop1R1^{KO/KO}$: same as 8C
9A, 9B, 9C, 9D	same as 8A

Construction of UAS-Pink Flamindo and UAS-ExRai-AKAR2

The Pink Flamindo cDNA was amplified by PCR from the plasmid (provided by Kitaguchi, Addgene plasmid #102356). The amplified fragment was then integrated into the 20xUAS vector originating from pJFRC7-20xUAS-IVS-mCD8::GFP (Pfeiffer, Addgene plasmid #26220) by In-Fusion recombinase (Clontech Laboratories). The ExRai-AKAR2 cDNA codon was optimized for Drosophila melanogaster (Eurofins

702 Genomics), and the resulting synthesized cDNA was cloned into the 20xUAS vector

703 described above.

704

705 **Live imaging**

706 **Chemicals**

707 Saline (103 mM NaCl, 3 mM KCl, 10 mM trehalose, 10 mM D-glucose, 26 mM

708 $NaHCO_3$, 1 mM NaH_2PO_4, 1.5 mM $CaCl_2$_$2H_2O$, 4 mM $MgCl_2$_$6H_2O$, 9 mM sucrose,

709 and 5 mM HEPES, (osmolarity adjusted to 270–280 mol/kg), Mineral oil (Fisher

710 Scientific, Fair Lawn, NJ, USA, Cat# O1214), 4-methylcyclohexanol, MCH (Cat#

711 66360, 98%>purity, Fluka, Sigma-Aldrich, St. Louis, MO, USA), 3-octanol, OCT (Cat#

712 74870, 95%>purity, Fluka, Sigma-Aldrich, St. Louis, MO, USA), Apple cider vinegar,

713 ACV (Mizkan jun-ringo-su, Mizkan holdings, Japan, ASIN#B000H2SCTW), Forskolin,

714 Fsk (Tokyo Chemical Industry, Cat# F0855), and Ethanol (Fujifilm Wako, Japan, Cat#

715 054-00466).

716

717 **Fly preparation**

718 Unless otherwise specified, female flies aged 5-16 days were used. A fly was mounted

719 on a custom-made imaging dish immediately after anesthetization by CO_2 gas spray for
720 3–5 s. The head capsule and dorsal thorax were secured to the dish by light-curing
721 glue (DYMAX Medical Adhesive, 1204-M-SC, USA). The proboscis was also glued
722 onto the capsule to reduce brain movement. A window on the top of the head capsule
723 was opened using sharp forceps (Corte Instruments, USA) and a thin injection needle
724 in saline. Air sacs and fat bodies were carefully removed, and muscle 16 was cut using
725 forceps to avoid excessive brain movements during imaging.
726
727 **Olfactory stimulation**
728 Odors were delivered with a custom-made, 8-channel olfactometer controlled by a
729 custom LabVIEW application (National Instruments). While a fly was mounted under
730 the microscope, a constant stream of pure air (0.4 L/min) was directed toward it. Thirty
731 mL of odor solution was placed in a 100 ml glass bottle (Duran, Cat# TGK 371-05-20-
732 03) with an Omnifit GL45 bottle cap (Diba Omnifit, Cat# OM4212), PTFE tube (Cat#
733 BLS181033, ⅛” x 2.4mm), and USL-PTFE joint (OOU-095-7x1/8”, custom-made, 7mm
734 x ⅛”, http//www.u-s-l.co.jp). All odorants except for ACV were diluted 1 : 10 vol/vol in
735 mineral oil. ACV was diluted 1 : 10 vol/vol in Milli-Q water. After a stimulation trigger, a
736 solenoid valve redirects a portion of the air stream through the headspace of the glass

737 bottle for 3 s. Two mass flow controllers (SEC-E40, HORIBA STEC, Japan) were used
738 in parallel to regulate the flow of pure air and odors. The odor stream rejoined the pure
739 air stream 40 cm from the end of the odor delivery tube (4 mm in diameter). The odor
740 was released from a position 5 mm in front of the fly at a flow rate of 0.4 L/min.
741 Subsequently, it was collected through a tube (3 mm in diameter) located 15 mm
742 behind the fly at a flow rate of 2 L/min, using a vacuum pump (ULVAC DA-20D,
743 ULVAC KIKO, Inc.) equipped with a charcoal filter. The intervals between odor
744 exposures were at least 60 seconds.
745
746 **Electric shock delivery**
747 A fly was subjected to electric stimulation by positioning one end of a platinum wire at
748 the base of its legs and the other end at the abdominal region, using a
749 micromanipulator (MNM-25, Narishige, Tokyo, Japan). At the time point 17.5 seconds
750 from the commencement of the recording, a 60-volt electric shock generated with an
751 Electric Stimulator (SEN-3401, Nihon Kohden, Japan) and Isolator (SS-203J, Nihon
752 Kohden, Japan) was administered to the fly for a duration of 10 milliseconds. In the
753 context of pairing odor and electric shock, electric stimulation was applied after a delay
754 of 1.5 seconds following the initiation of a 3-second odor presentation. The

755 administration of the shock was verified by observing the movements of the legs and
756 the occurrence of abdominal cramps, using a CCD camera (STC-TB33USB, Omron
757 Sentech, Tokyo, Japan).
758
759 **Forskolin bath application**
760 Forskolin, a compound of interest, was dissolved in a solution containing saline and
761 100% EtOH in a 3:1 ratio, to make a stock solution with a 5 mM Forskolin
762 concentration. From this stock solution, a working solution was prepared by dilution
763 with saline to achieve a concentration of 100 μM Forskolin in saline with 0.5% EtOH.
764 As a control, saline with 0.5% EtOH was used. For live imaging, the standard saline
765 solution was removed, leaving a small remaining volume of 50 μl on the objective and
766 dish. Then, a syringe containing saline with 0.5% EtOH was connected to the dish,
767 allowing the space between the objective and dish to be filled. The recording was
768 performed for a duration of 4 minutes. Subsequently, the saline with 0.5% EtOH was
769 replaced with 1 mL of the 100 μM Forskolin solution in saline with 0.5% EtOH, and
770 another 4-minute recording was conducted. During this time, the responses to odors
771 were recorded. At the end of the recordings, the 100 μM Forskolin solution in saline
772 with 0.5% EtOH was washed out by replacing it with the standard saline solution four

773 times, and the responses to odors under the wash-out conditions were also recorded.

774

775 **Two-photon laser microscopy**

776 For *in vivo* two-photon imaging, we employed a two-photon microscope (Olympus
777 FVMPE-RS; Olympus, Tokyo, Japan) equipped with a water-immersion objective lens
778 (XLPLN25XWM, 25x N.A. 1.05), a titanium:sapphire pulsed laser (INSIGHT DS DUAL-
779 OL; Spectra-Physics, Santa Clara, CA, USA), and a Galvano Scanner to facilitate live
780 imaging. The emitted light was collected using GaAsP photomultiplier detectors with
781 495-540 nm and 575-645 nm bandpass filters (FV30-FGR). G-CaMP6f and G-Flamp1
782 were excited at 925 nm, GRAB_DA2m, GRAB_ACh3.0, and ExRai-AKAR2 were
783 excited at 980 nm, while jRGECO1b and Pink Flamindo were excited at 1040 nm.
784 Using the Olympus FV31S-SW imaging software, we acquired time series images with
785 different dimensions: 400-430 x 130-120 pixels (0.14-0.19 μm/pixel, γ1-γ2 zoom in
786 Figure 3), 275-320 x 155-140 (0.33-0.50 μm/pixel, γ1-γ5 in Figures 1, 2, 4, 5, 6, and 7),
787 and 180-250 x 150-165 (0.15-0.20 μm/pixel, α'3/α3 in Figure 1). The acquisition was
788 performed at a frame rate of either 333 or 500 ms/frame in a sequential line scan
789 mode, ensuring that the time difference between acquiring images for channels 1 and 2
790 was less than 2 ms. By default, images were acquired for a duration of 40 s to capture

791 the response to each stimulus and were saved for subsequent image processing. The
792 solenoid valve for odor stimulation was activated 15 s after the start of each recording,
793 and delivered the odor for a duration of 3 s, corresponding to frames #46-54 (333
794 ms/frame) or #31-36 (500 ms/frame). For quantitative analysis, ΔF/F0 images of peak
795 responses were generated by averaging frames #51-65 (333 ms/frame) or frames #35-
796 44 (500 ms/frame). The experimental flies, which were housed in vials with food, were
797 transferred to an imaging room maintained at 22°C at least two days prior to the
798 imaging experiments.
799
800 **Image analysis**
801 The image analysis was conducted as described previously (Hiroi et al., 2013), with
802 several modifications. The images within each recording were stabilized using the
803 template matching plugin of Fiji (ImageJ). To mitigate the impacts of detector noise and
804 uncorrected movement, all reporter signals underwent an initial processing step
805 employing a median filter (with a radius of 1 pixel). For the images obtained from the
806 same fly, after stabilization, a template matching technique was utilized for alignment.
807 Subsequently, the ΔF values were computed based on the average (F0) of the one-
808 second interval following the opening of the valve (specifically, 15 seconds after the

809 start of the recording). It is important to note that the median filter (with a radius of 1
810 pixel) was once again applied during this stage. To identify the KC region (also known
811 as the region of interest, ROI), Li's binarizing algorithm was applied to the averaged
812 signal intensity across the entire duration of each recording, using Fiji. Regions of
813 interest (ROIs) for each compartment were first manually identified, using the
814 anatomical characteristics as a guide. The demarcation between the γ3 and γ4
815 compartments was occasionally challenging to determine, and it was pragmatically
816 established that the border lies within the middle of the regions assigned to the γ3 and
817 γ4 compartments. The drawing and preservation of ROIs, as well as the measurement
818 of ΔF/F0, were performed in a semi-automated manner using both built-in and custom-
819 written macro routines in Fiji. Furthermore, additional image processing tasks, such as
820 correlation testing and temporal dynamics plotting, were executed using MATLAB
821 scripts.
822
823 **Scatter Plot Analysis**
824 We computed the mean ΔF/F0 values of calcium and cAMP transients within the
825 designated γ1 and γ2 compartments for each pixel during the 1 to 6 seconds following
826 the delivery of OCT or OCT + electrical shock, employing the identical method outlined

827 in the preceding image analysis section. These calculated values were then plotted on
828 a scatter plot, with calcium represented on the X-axis and cAMP on the Y-axis for each
829 pixel. To assess the linearity of the relationship, we conducted a linear regression
830 analysis on the scatter plot and determined the R^2 value. To simulate the potential
831 maximum linearity between the two values in our experimental setup, we created an
832 additional scatter plot. We divided the dataset obtained from calcium transients into two
833 groups, based on whether the frame number was odd or even. Then, we plotted the
834 values from the odd-numbered frames on the X-axis and the values from the even-
835 numbered frames on the Y-axis. The processes of acquiring data, generating scatter
836 plots, applying linear regression analysis, and calculating R^2 values were all executed
837 utilizing the MATLAB software.
838
839 **Statistics**
840 Statistical analyses were conducted using the Prism 9 software (GraphPad). All tests
841 were non-parametric, two-tailed, and the confidence levels were set at $\alpha = 0.05$. The
842 figure legends provide the p values and specify the comparisons made for each
843 experiment, unless otherwise indicated. The bar graphs display the means ± SEM for
844 the data.

Acknowledgements

We thank Yuuichi Iino, Joshua Johansen, Hokto Kazama, Satoshi Kida, Tom Kornberg, Minoru Saitoe, and Kazumichi Shimizu for their valuable comments. We are grateful to Atsushi Miyajima for providing access to the Ti:sapphire laser. We also thank H. Takishita and M. Sato for excellent help with fly husbandry. We would also like to thank Yoshinori Aso, Jun Chu, Yulong Li, Taro Ueno, the Kyoto DGRC, the NIG Stock Center, the Bloomington Stock Center, and the Janelia Research Campus/HHMI for fly stocks. This work was supported by grants from the Ministry of Education, Culture, Sports, Science and Technology (17K17681 and 19K16254 to T.A., 21K06388 to D.Y. and 19H03268 to T.T., A.T. and D.Y.) and the Takeda Science Foundation to T.T.

Author contributions: T.A., D.Y. and T.T. designed the research; T.A. performed live imaging and statistical analyses; D.Y. constructed transgenes and performed live imaging in the early phase; M.H. developed an imaging data acquisition and analysis system; Y.M. conducted genetic and histological experiments; Y.U. performed statistical analyses. T.A., D.Y. and T.T. wrote the manuscript.

Competing interest

The authors declare that no competing interests exist.

References

Abrams TW, Kandel ER. 1988. Is contiguity detection in classical conditioning a system or a cellular property? Learning in Aplysia suggests a possible molecular site. *Trends Neurosci* **11**:128–135. doi:10.1016/0166-2236(88)90137-3

Adel M, Chen N, Zhang Y, Reed ML, Quasney C, Griffith LC. 2022. Pairing-dependent plasticity in a dissected fly brain is input-specific and requires synaptic CaMKII enrichment and nighttime sleep. *J Neurosci* JN-RM-0144-22. doi:10.1523/jneurosci.0144-22.2022

Aso Y, Herb A, Ogueta M, Siwanowicz I, Templier T, Friedrich AB, Ito K, Scholz H, Tanimoto H. 2012. Three dopamine pathways induce aversive odor memories with different stability. *PLoS genetics* **8**:e1002768. doi:10.1371/journal.pgen.1002768

Berry JA, Cervantes-Sandoval I, Nicholas EP, Davis RL. 2012. Dopamine is required for learning and forgetting in Drosophila. *Neuron* **74**:530–542. doi:10.1016/j.neuron.2012.04.007

Bilz F, Geurten BRH, Hancock CE, Widmann A, Fiala A. 2020. Visualization of a Distributed Synaptic Memory Code in the Drosophila Brain. *Neuron*. doi:10.1016/j.neuron.2020.03.010

Burke CJ, Huetteroth W, Owald D, Perisse E, Krashes MJ, Das G, Gohl D, Silies M, Certel S, Waddell S. 2012. Layered reward signalling through octopamine and dopamine in Drosophila. *Nature* **492**:433–437. doi:10.1038/nature11614

Carew T, Walters E, Kandel E. 1981. Classical conditioning in a simple withdrawal reflex in Aplysia californica. *J Neurosci* **1**:1426–1437. doi:10.1523/jneurosci.01-12-01426.1981

Cassenaer S, Laurent G. 2012. Conditional modulation of spike-timing-dependent plasticity for olfactory learning. *Nature* **482**:47–52. doi:10.1038/nature10776

888 Cervantes-Sandoval I, Phan A, Chakraborty M, Davis RL, Vijayraghavan K. 2017. Reciprocal
889 synapses between mushroom body and dopamine neurons form a positive feedback loop
890 required for learning. *eLife* **6**:e23789. doi:10.7554/elife.23789

891 Chen N, Zhang Y, Adel M, Kuklin EA, Reed ML, Mardovin JD, Bakthavachalu B,
892 VijayRaghavan K, Ramaswami M, Griffith LC. 2022. Local translation provides the
893 asymmetric distribution of CaMKII required for associative memory formation. *Curr Biol*.
894 doi:10.1016/j.cub.2022.04.047

895 Crittenden JR, Skoulakis EMC, Han K-A, Kalderon D, Davis RL. 1998. Tripartite Mushroom
896 Body Architecture Revealed by Antigenic Markers. *Learn Memory* **5**:38-51.
897 doi:10.1101/lm.5.1.38

898 Dana H, Mohar B, Sun Y, Narayan S, Gordus A, Hasseman JP, Tsegaye G, Holt GT, Hu A,
899 Walpita D, Patel R, Macklin JJ, Bargmann CI, Ahrens MB, Schreiter ER, Jayaraman V,
900 Looger LL, Svoboda K, Kim DS. 2016. Sensitive red protein calcium indicators for imaging
901 neural activity. *Elife* **5**:e12727. doi:10.7554/elife.12727

902 Davis RL. 1993. Mushroom bodies and drosophila learning. *Neuron* **11**:1-14.
903 doi:10.1016/0896-6273(93)90266-t

904 Gervasi N, Tchénio P, Preat T. 2010. PKA dynamics in a Drosophila learning center:
905 coincidence detection by rutabaga adenylyl cyclase and spatial regulation by dunce
906 phosphodiesterase. *Neuron* **65**:516-529. doi:10.1016/j.neuron.2010.01.014

907 Gu H, O'Dowd DK. 2006. Cholinergic synaptic transmission in adult Drosophila Kenyon cells
908 in situ. *The Journal of neuroscience : the official journal of the Society for Neuroscience*
909 **26**:265-272. doi:10.1523/jneurosci.4109-05.2006

910 Handler A, Graham TGW, Cohn R, Morantte I, Siliciano AF, Zeng J, Li Y, Ruta V. 2019.
911 Distinct Dopamine Receptor Pathways Underlie the Temporal Sensitivity of Associative
912 Learning. *Cell* **178**:60-75. doi:10.1016/j.cell.2019.05.040

913 Harada K, Ito M, Wang X, Tanaka M, Wongso D, Konno A, Hirai H, Hirase H, Tsuboi T,
914 Kitaguchi T. 2017. Red fluorescent protein-based cAMP indicator applicable to
915 optogenetics and in vivo imaging. *Sci Rep-uk* **7**:7351. doi:10.1038/s41598-017-07820-6

916 Heisenberg M. 2003. Mushroom body memoir: from maps to models. *Nature reviews*
917 *Neuroscience* **4**:266–275. doi:10.1038/nrn1074

918 Hige T, Aso Y, Rubin GM, Turner GC. 2015. Plasticity-driven individualization of olfactory
919 coding in mushroom body output neurons. *Nature* **526**:258–262. doi:10.1038/nature15396

920 Hiroi M, Ohkura M, Nakai J, Masuda N, Hashimoto K, Inoue K, Fiala A, Tabata T. 2013.
921 Principal component analysis of odor coding at the level of third-order olfactory neurons
922 in Drosophila. *Genes to cells : devoted to molecular & cellular mechanisms*.
923 doi:10.1111/gtc.12094

924 Honegger KS, Campbell RAA, Turner GC. 2011. Cellular-resolution population imaging
925 reveals robust sparse coding in the Drosophila mushroom body. *The Journal of*
926 *neuroscience* **31**:11772–11785. doi:10.1523/jneurosci.1099-11.2011

927 Huang C, Luo J, Woo SJ, Roitman L, Li J, Pieribone V, Kannan M, Vasan G, Schnitzer M.
928 2022. Dopamine signals integrate innate and learnt valences to regulate memory
929 dynamics. *Research Square*. doi:10.21203/rs.3.rs-1915648/v1

930 Jacob PF, Vargas-Gutierrez P, Okray Z, Vietti-Michelina S, Felsenberg J, Waddell S. 2021.
931 Prior experience conditionally inhibits the expression of new learning in Drosophila. *Curr*
932 *Biol* **31**:3490–3503. doi:10.1016/j.cub.2021.05.056

933 Karuppudurai T, Lin T-Y, Ting C-Y, Pursley R, Melnattur KV, Diao F, White BH, Macpherson
934 LJ, Gallio M, Pohida T, Lee C-H. 2014. A Hard-Wired Glutamatergic Circuit Pools and
935 Relays UV Signals to Mediate Spectral Preference in Drosophila. *Neuron* **81**:603–615.
936 doi:10.1016/j.neuron.2013.12.010

937 Kato A, Ohta K, Okanoya K, Kazama H. 2023. Dopaminergic neurons dynamically update
938 sensory values during olfactory maneuver. *Cell Rep* 113122.
939 doi:10.1016/j.celrep.2023.113122

940 Kim Y-C, Lee H-G, Han K-A. 2007. D1 dopamine receptor dDA1 is required in the
941 mushroom body neurons for aversive and appetitive learning in Drosophila. *The Journal*
942 *of neuroscience : the official journal of the Society for Neuroscience* **27**:7640–7647.
943 doi:10.1523/jneurosci.1167-07.2007

König C, Khalili A, Niewalda T, Gao S, Gerber B. 2019. An optogenetic analogue of second-order reinforcement in Drosophila. *Biol Letters* **15**:20190084. doi:10.1098/rsbl.2019.0084

Levin LR, Han PL, Hwang PM, Feinstein PG, Davis RL, Reed RR. 1992. The Drosophila learning and memory gene rutabaga encodes a Ca2+/Calmodulin-responsive adenylyl cyclase. *Cell* **68**:479–489.

Li F, Lindsey JW, Marin EC, Otto N, Dreher M, Dempsey G, Stark I, Bates AS, Pleijzier MW, Schlegel P, Nern A, Takemura S-Y, Eckstein N, Yang T, Francis A, Braun A, Parekh R, Costa M, Scheffer LK, Aso Y, Jefferis GS, Abbott LF, Litwin-Kumar A, Waddell S, Rubin GM. 2020. The connectome of the adult Drosophila mushroom body provides insights into function. *eLife* **9**. doi:10.7554/elife.62576

Liu C, Goel P, Kaeser PS. 2021. Spatial and temporal scales of dopamine transmission. *Nat Rev Neurosci* **22**:345–358. doi:10.1038/s41583-021-00455-7

Liu C, Plaçais P-Y, Yamagata N, Pfeiffer BD, Aso Y, Friedrich AB, Siwanowicz I, Rubin GM, Preat T, Tanimoto H. 2012. A subset of dopamine neurons signals reward for odour memory in Drosophila. *Nature* **488**:512–516. doi:10.1038/nature11304

Livingstone MS. 1985. Genetic dissection of Drosophila adenylate cyclase. *Proc National Acad Sci* **82**:5992–5996. doi:10.1073/pnas.82.17.5992

Livingstone MS, Sziber PP, Quinn WG. 1984. Loss of calcium/calmodulin responsiveness in adenylate cyclase of rutabaga, a Drosophila learning mutant. *Cell* **37**:205–215. doi:10.1016/0092-8674(84)90316-7

Manoim JE, Davidson D, Weiss S, Hige T, Parnas M. 2022. Lateral Axonal Modulation Is Required for Stimulus-Specific Olfactory Conditioning in Drosophila. *Ssrn Electron J.* doi:10.2139/ssrn.4120768

Mao Z, Davis RL. 2009. Eight different types of dopaminergic neurons innervate the Drosophila mushroom body neuropil: anatomical and physiological heterogeneity. *Frontiers in neural circuits* **3**:5. doi:10.3389/neuro.04.005.2009

McGuire SE, Le PT, Osborn AJ, Matsumoto K, Davis RL. 2003. Spatiotemporal rescue of memory dysfunction in Drosophila. *Science (New York, NY)* **302**:1765–1768. doi:10.1126/science.1089035

973 Miyashita T, Murakami K, Kikuchi E, Ofusa K, Mikami K, Endo K, Miyaji T, Moriyama S, Konno
974 K, Muratani H, Moriyama Y, Watanabe M, Horiuchi J, Saitoe M. 2023. Glia transmit
975 negative valence information during aversive learning in Drosophila. *Science*
976 **382**:eadf7429. doi:10.1126/science.adf7429

977 Mons N, Guillou JL, Jaffard R. 1999. The role of Ca 2+ /calmodulin-stimulable adenylyl
978 cyclases as molecular coincidence detectors in memory formation. *Cellular and Molecular*
979 *Life Sciences (CMLS)* **55**:525-533. doi:10.1007/s000180050311

980 Nair AG, Bhalla US, Kotaleski JH. 2016. Role of DARPP-32 and ARPP-21 in the Emergence
981 of Temporal Constraints on Striatal Calcium and Dopamine Integration. *Plos Comput Biol*
982 **12**:e1005080. doi:10.1371/journal.pcbi.1005080

983 Noyes NC, Davis RL. 2023. Innate and learned odor-guided behaviors utilize distinct
984 molecular signaling pathways in a shared dopaminergic circuit. *Cell Reports* **42**:112026.
985 doi:10.1016/j.celrep.2023.112026

986 Ocorr KA, Walters ET, Byrne JH. 1985. Associative conditioning analog selectively increases
987 cAMP levels of tail sensory neurons in Aplysia. *Proc National Acad Sci* **82**:2548-2552.
988 doi:10.1073/pnas.82.8.2548

989 Pribbenow C, Chen Y, Heim M-M, Laber D, Reubold S, Reynolds E, Balles I, Alquicira TFV,
990 Suárez-Grimalt R, Scheunemann L, Rauch C, Matkovic T, Rösner J, Lichtner G,
991 Jagannathan SR, Owald D. 2022. Postsynaptic plasticity of cholinergic synapses
992 underlies the induction and expression of appetitive and familiarity memories in
993 Drosophila. *Elife* **11**:e80445. doi:10.7554/elife.80445

994 Qiao J, Yang S, Geng H, Yung W-H, Ke Y. 2022. Input-timing-dependent plasticity at
995 incoming synapses of the mushroom body facilitates olfactory learning in Drosophila.
996 *Curr Biol*. doi:10.1016/j.cub.2022.09.054

997 Rescorla RA. 1988. Behavioral Studies of Pavlovian Conditioning. *Annu Rev Neurosci*
998 **11**:329-352. doi:10.1146/annurev.ne.11.030188.001553

999 Riemensperger T, Völler T, Stock P, Buchner E, Fiala A. 2005. Punishment prediction by
1000 dopaminergic neurons in Drosophila. *Current biology* **15**:1953-1960.
1001 doi:10.1016/j.cub.2005.09.042

1002 Rubin GM, Aso Y. 2024. New genetic tools for mushroom body output neurons in Drosophila.
1003 *eLife* **12**. doi:10.7554/elife.90523

1004 Saitoe. 2021. A non-canonical on-demand dopaminergic transmission underlying olfactory
1005 aversive learning. *Neurosci Res* **178**:1-9. doi:10.1016/j.neures.2021.12.008

1006 Scheunemann L, Jost E, Richlitzki A, Day JP, Sebastian S, Thum AS, Efetova M, Davies S-
1007 A, Schwärzel M. 2012. Consolidated and Labile Odor Memory Are Separately Encoded
1008 within the Drosophila Brain. *The Journal of neuroscience : the official journal of the*
1009 *Society for Neuroscience* **32**:17163-17171. doi:10.1523/jneurosci.3286-12.2012

1010 Schwaerzel M, Monastirioti M, Scholz H, Friggi-Grelin F, Birman S, Heisenberg M. 2003.
1011 Dopamine and octopamine differentiate between aversive and appetitive olfactory
1012 memories in Drosophila. *The Journal of neuroscience : the official journal of the Society*
1013 *for Neuroscience* **23**:10495-10502.

1014 Shuai Y, Hu Y, Qin H, Campbell RAA, Zhong Y. 2011. Distinct molecular underpinnings of
1015 Drosophila olfactory trace conditioning. *Proceedings of the National Academy of*
1016 *Sciences of the United States of America*. doi:10.1073/pnas.1107489109

1017 Shuai Y, Sammons M, Sterne G, Hibbard K, Yang H, Yang C-P, Managan C, Siwanowicz I,
1018 Lee T, Rubin GM, Turner G, Aso Y. 2024a. Driver lines for studying associative learning in
1019 Drosophila. doi:10.7554/elife.94168.1

1020 Shuai Y, Sammons M, Sterne G, Hibbard K, Yang H, Yang C-P, Managan C, Siwanowicz I,
1021 Lee T, Rubin GM, Turner G, Aso Y. 2024b. Driver lines for studying associative learning in
1022 Drosophila. doi:10.7554/elife.94168.1

1023 Siju KP, Stih V, Aimon S, Gjorgjieva J, Portugues R, Kadow ICG. 2020. Valence and State-
1024 Dependent Population Coding in Dopaminergic Neurons in the Fly Mushroom Body.
1025 *Current Biology* **30**:2104-2115.e4. doi:10.1016/j.cub.2020.04.037

1026 Stahl A, Noyes NC, Boto T, Botero V, Broyles CN, Jing M, Zeng J, King LB, Li Y, Davis RL,
1027 Tomchik SM. 2022. Associative learning drives longitudinally-graded presynaptic
1028 plasticity of neurotransmitter release along axonal compartments. *Elife* **11**.
1029 doi:10.7554/elife.76712

1030 Sugamori KS, Demchyshyn LL, McConkey F, Forte MA, Niznik HB. 1995. A primordial
1031 dopamine D1-like adenylyl cyclase-linked receptor from Drosophila melanogaster
1032 displaying poor affinity for benzazepines. *Febs Lett* **362**:131–138. doi:10.1016/0014-
1033 5793(95)00224-w

1034 Sun F, Zhou J, Dai B, Qian T, Zeng J, Li X, Zhuo Y, Zhang Y, Wang Y, Qian C, Tan K, Feng J,
1035 Dong H, Lin D, Cui G, Li Y. 2020. Next-generation GRAB sensors for monitoring
1036 dopaminergic activity in vivo. *Nat Methods* **17**:1156–1166. doi:10.1038/s41592-020-
1037 00981-9

1038 Sweeney ST, Broadie K, Keane J, Niemann H, O'Kane CJ. 1995. Targeted expression of
1039 tetanus toxin light chain in Drosophila specifically eliminates synaptic transmission and
1040 causes behavioral defects. *Neuron* **14**:341–351. doi:10.1016/0896-6273(95)90290-2

1041 Tomchik SM, Davis RL. 2009. Dynamics of learning-related cAMP signaling and stimulus
1042 integration in the Drosophila olfactory pathway. *Neuron* **64**:510–521.
1043 doi:10.1016/j.neuron.2009.09.029

1044 Tully T. 1987. Drosophila learning and memory revisited. *Trends Neurosci* **10**:330–335.
1045 doi:10.1016/0166-2236(87)90090-7

1046 Tully T, Quinn WG. 1985. Classical conditioning and retention in normal and
1047 mutantDrosophila melanogaster. *J Comp Physiology* **157**:263–277.
1048 doi:10.1007/bf01350033

1049 Ueno K, Suzuki E, Naganos S, Ofusa K, Horiuchi J, Saitoe M. 2017. Coincident postsynaptic
1050 activity gates presynaptic dopamine release to induce plasticity in Drosophila mushroom
1051 bodies. *eLife* **6**:156. doi:10.7554/elife.21076

1052 Ueoka Y, Hiroi M, Abe T, Tabata T. 2017. Suppression of a single pair of mushroom body
1053 output neurons in Drosophila triggers aversive associations. *FEBS open bio* **7**:562–576.
1054 doi:10.1002/2211-5463.12203

1055 Wang L, Wu C, Peng W, Zhou Z, Zeng J, Li X, Yang Y, Yu S, Zou Y, Huang M, Liu C, Chen Y,
1056 Li Yi, Ti P, Liu W, Gao Y, Zheng W, Gao S, Lu Z, Ren P-G, Ng HL, He J, Chen S, Xu M, Li
1057 Yulong, Chu J. 2022. A high-performance genetically encoded fluorescent indicator for in
1058 vivo cAMP imaging. *Biorxiv* 2022.02.27.482140. doi:10.1101/2022.02.27.482140

1059 Yamada D, Bushey D, Li F, Hibbard KL, Sammons M, Funke J, Litwin-Kumar A, Hige T, Aso
1060 Y. 2023. Hierarchical architecture of dopaminergic circuits enables second-order
1061 conditioning in Drosophila. *Elife* **12**:e79042. doi:10.7554/elife.79042

1062 Yamada D, Davidson AM, Hige T. 2024. Cyclic nucleotide-induced bidirectional long-term
1063 synaptic plasticity in Drosophila mushroom body. *J Physiol*. doi:10.1113/jp285745

1064 Yamagata N, Hiroi M, Kondo S, Abe A, Tanimoto H. 2016. Suppression of Dopamine Neurons
1065 Mediates Reward **14**:e1002586. doi:10.1371/journal.pbio.1002586

1066 Yamazaki D, Hiroi M, Abe T, Shimizu K, Minami-Ohtsubo M, Maeyama Y, Horiuchi J, Tabata
1067 T. 2018. Two Parallel Pathways Assign Opposing Odor Valences during Drosophila
1068 Memory Formation. *Cell reports* **22**:2346-2358. doi:10.1016/j.celrep.2018.02.012

1069 Yovell Y, Kandel ER, Dudai Y, Abrams TW. 1992. A Quantitative Study of the
1070 Ca2+/Calmodulin Sensitivity of Adenylyl Cyclase in Aplysia, Drosophila, and Rat. *J*
1071 *Neurochem* **59**:1736-1744. doi:10.1111/j.1471-4159.1992.tb11005.x

1072 Zars T, Fischer M, Schulz R, Heisenberg M. 2000. Localization of a Short-Term Memory in
1073 Drosophila. *Science (New York, NY)* **288**:672-675. doi:10.1126/science.288.5466.672

1074 Zeng J, Li X, Zhang R, Lv M, Wang Y, Tan K, Xia X, Wan J, Jing M, Zhang X, Li Yu, Yang Y,
1075 Wang L, Chu J, Li Yan, Li Yulong. 2023. Local 5-HT signaling bi-directionally regulates
1076 the coincidence time window for associative learning. *Neuron*.
1077 doi:10.1016/j.neuron.2022.12.034

1078 Zhang J-F, Liu B, Hong I, Mo A, Roth RH, Tenner B, Lin W, Zhang JZ, Molina RS, Drobizhev
1079 M, Hughes TE, Tian L, Huganir RL, Mehta S, Zhang J. 2021. An ultrasensitive biosensor
1080 for high-resolution kinase activity imaging in awake mice. *Nat Chem Biol* **17**:39-46.
1081 doi:10.1038/s41589-020-00660-y

1082

1083

1084

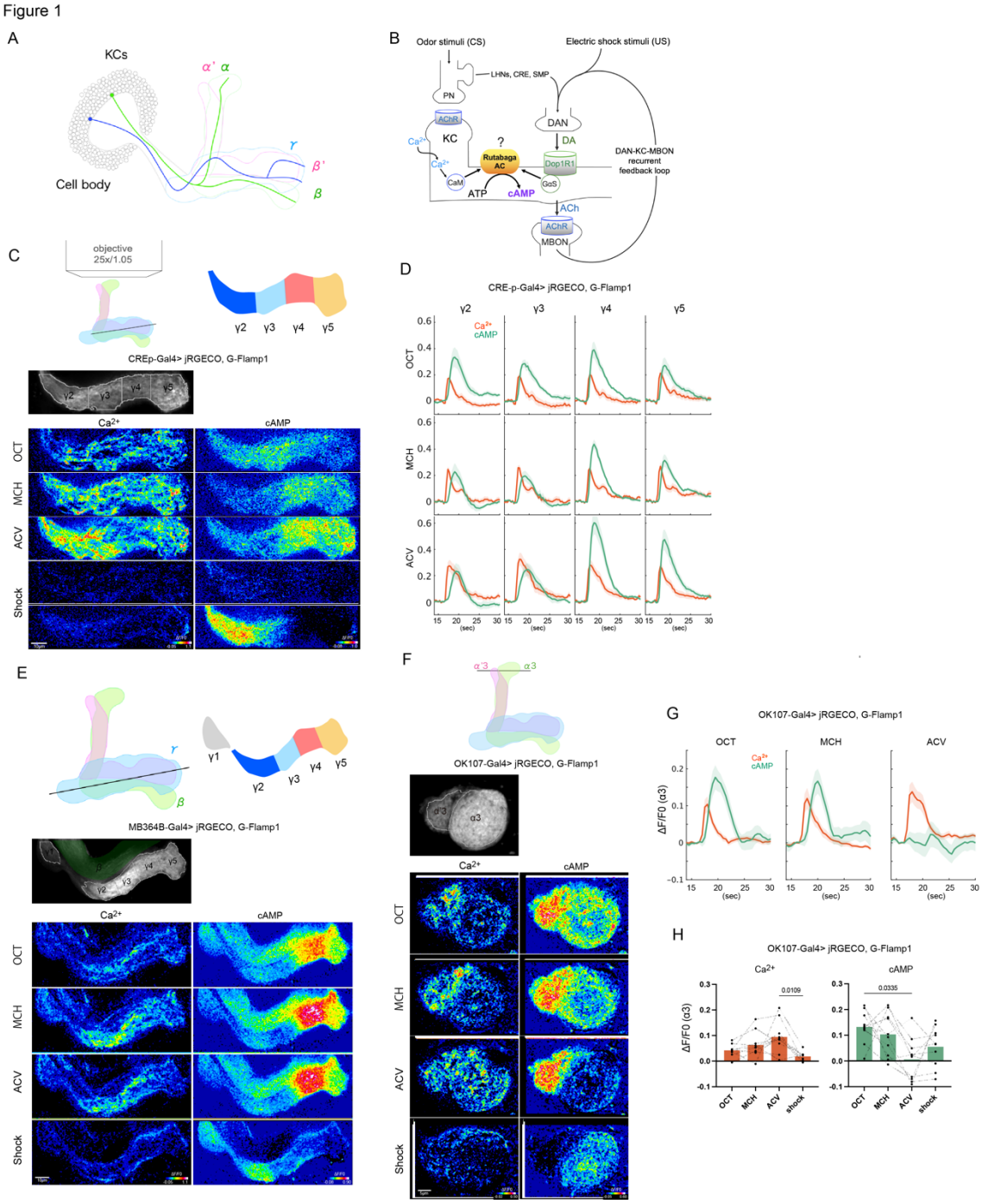

Figure 1. Odor presentation evokes cAMP elevation in a broad population of KCs independently of calcium responses. (**A**) Schematic of Kenyon cells (KCs), referred to Figure 1A (Bilz et al., 2020). The cell body, the α/β, α'/β' and γ lobes, and the α/β and γ KCs are depicted. (**B**) Schematic of the role of the Rutabaga adenylyl cyclase (Rut AC)

1090 as the coincidence detector. KCs innervated by PPL1 DANs. The odor acquisition (CS)
1091 activates acetylcholine signaling and elevates calcium concentrations through voltage-
1092 gated calcium channels. PPL1 DANs integrate odor information and noxious stimuli
1093 (US) such as electric shock through regions including the lateral horns (LHNs), Crepine
1094 (CRE), and superior medial protocerebrum (SMP)(Kato et al., 2023). DANs activities
1095 are also regulated by the DAN-KC-MBON recurrent feedback loop (Adel and Griffith,
1096 2021). The CS and US pathways can converge on the Rut AC, which is synergistically
1097 activated by the calcium/calmodulin complex and the Gα subunit of the G-protein
1098 complex coupled to the D1-like dopamine receptor Dop1R1. (**C**) Schematic
1099 representation of *in vivo* imaging of KCs. The objective and frontal view of the KCs
1100 along with the focal plane (upper left), and the dorsal view of γ KCs with color-coded
1101 γ2-5 compartments (upper right) are shown. Two-photon live imaging was conducted
1102 on the γ2-γ5 compartments of KCs in flies expressing jRGECO1b and G-Flamp1,
1103 driven by the γCRE-p-GAL4 driver. Exemplary, finely resolved images are shown.
1104 Averaged calcium responses during a 40-second air exposure were used to show the
1105 regions of interest (ROIs) for each compartment, depicted in grayscale. Pseudocolor
1106 images of averaged peak responses (10 frames for 5 s) of calcium and cAMP during
1107 the presentations of 4-methylcyclohexanol (MCH), 3-octanol (OCT), apple cider

1108 vinegar (ACV), and electric shock (Shock, two bouts). All images in the present study
1109 were acquired using a dual-channel line-scanning mode. (**D**) The graph shows the
1110 changes in calcium (in red) and cAMP (in green) levels over 15-30 seconds in
1111 response to different odors (OCT, MCH, and ACV) in four γ lobe compartments (γ2-γ5)
1112 driven by the γ-CRE-p-GAL4 driver. The odors were presented by opening the solenoid
1113 valve between 15-18 seconds. Solid lines represent the average response from 8 flies,
1114 and shaded areas show the standard error of the mean (SEM). (**E**) The focal plane of
1115 live imaging for compartments γ1-γ5 is schematically presented (Upper panel). Two-
1116 photon live imaging on the γ1-γ5 compartments of KCs in flies expressing jRGECO1b
1117 and G-Flamp1, driven by the MB364B-GAL4 driver. Averaged calcium responses
1118 during a 40-second air exposure were utilized to show ROIs for each compartment,
1119 depicted in grayscale. The ΔF/F0 images of averaged peak responses (10 frames, 5 s)
1120 of calcium and cAMP during the presentations of MCH, OCT, ACV, and shock in
1121 compartments γ1-γ5 (lower panels). (**F**) The focal plane of live imaging for the α3/α'3
1122 compartments is schematically presented (upper panel). Two-photon live imaging on
1123 the α3/α'3 compartments of KCs in flies expressing jRGECO1b and G-Flamp1, driven
1124 by the OK107 driver. Averaged calcium responses during a 40-second air exposure
1125 were utilized to show ROIs for each compartment, depicted in grayscale. Magnified

1126 images of averaged peak ΔF/F0 responses (10 frames, 5 s) of calcium and cAMP in
1127 the α3 and α'3 compartments are shown. (**G**) The graph shows the changes in calcium
1128 (in red) and cAMP (in green) levels over 15-30 seconds in response to different odors
1129 (OCT, MCH, and ACV) in the α3 lobe compartment driven by the OK107-GAL4 driver.
1130 The odors were presented by opening the solenoid valve between 15-18 seconds.
1131 Solid lines represent the average response from 10 flies, and shaded areas show the
1132 standard error of the mean (SEM). ACV elicited the highest calcium response but the
1133 lowest cAMP response, compared to OCT and MCH. (**H**) The ΔF/F0 images, obtained by
1134 averaging the responses to odor stimuli over a duration of 5 seconds, corresponding to
1135 10 frames, were quantified. The plots of the α3 compartment derived from the same
1136 sample are connected with dashed lines. The bar graph illustrates the mean values. p-
1137 values are shown for comparisons where a significant difference was observed. Dunn's
1138 multiple comparisons test for all pairwise combinations, $p < 0.05$; $n = 10$.
1139

Figure 2

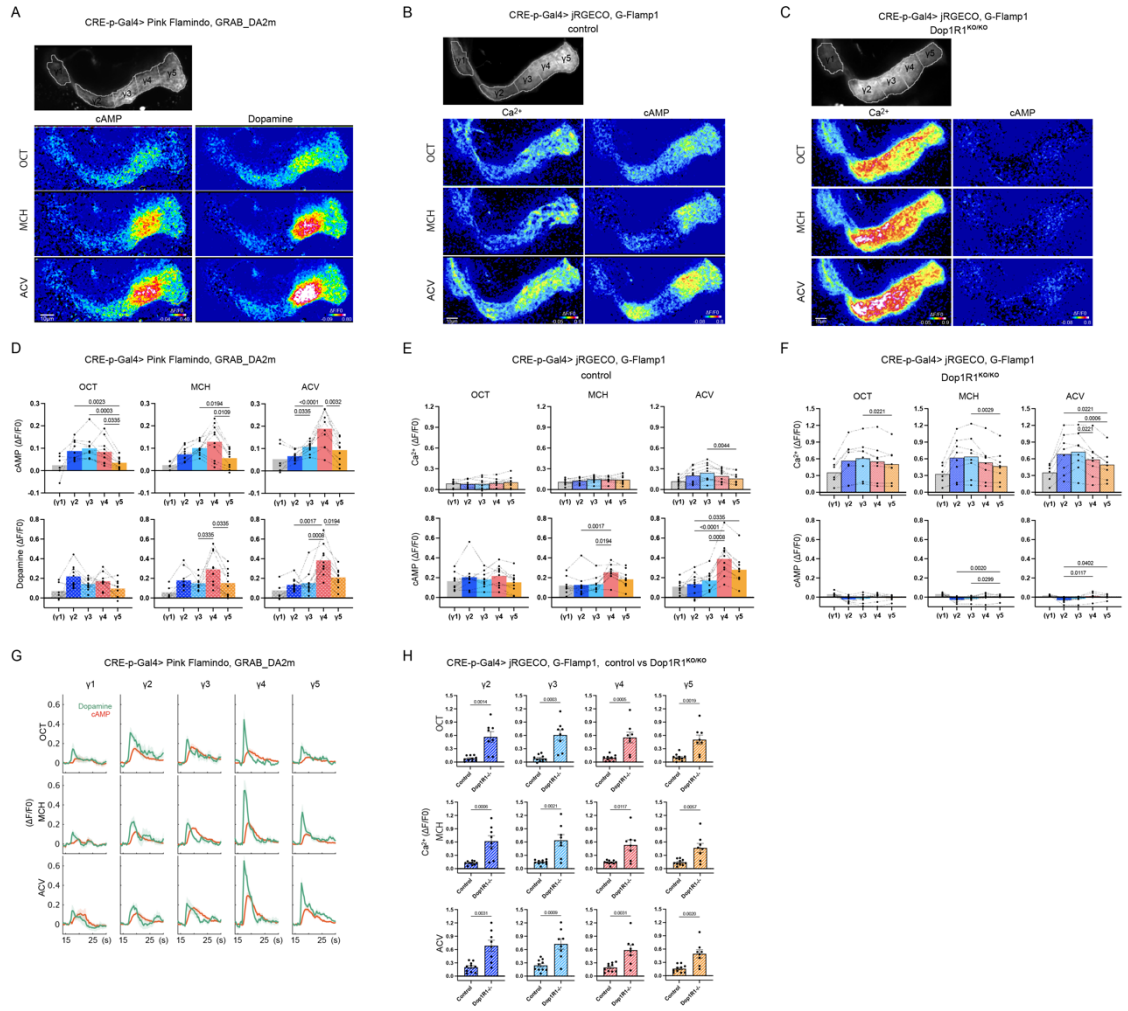

Figure 2. Dopamine induces cAMP synthesis. (**A**) Two-photon live imaging on γ1-γ5 compartments of KCs in flies expressing Pink Flamindo and GRAB_DA2m, driven by the γCRE-p-GAL4 driver. Averaged calcium responses during a 40-second air exposure were used to show ROIs for each compartment, depicted in grayscale. ΔF/F0 images of averaged peak responses (10 frames, 3.3 s) of cAMP and dopamine during the presentations of OCT, MCH and ACV. (**B,C**) Two-photon live imaging on the γ1-γ5 compartments of KCs in flies expressing jRGECO1b and G-Flamp1, driven by the

1148 γCRE-p-GAL4 driver of the genetic control flies (**B**) and the *Dop1R1* mutant flies (**C**).

1149 Averaged calcium responses during a 40-second air exposure were used to show

1150 ROIs for each compartment, depicted in grayscale. ΔF/F0 images of averaged peak

1151 responses (15 frames, 5 s) of calcium and cAMP during the presentations of OCT,

1152 MCH, and ACV. (**D**-**F**) The quantification of the ΔF/F0 images, obtained by averaging

1153 the responses of cAMP and dopamine (**D**), Ca^{2+} and cAMP (**E-F**) to odor stimuli. The

1154 plots of different compartments derived from the same sample are connected with

1155 dashed lines. The bar graph illustrates the mean values. γ1: n = 6, γ2-γ5: n = 10 (**D**),

1156 γ1: n = 9, γ2-γ5: n = 10 (**E**) and γ1, n = 6, γ2-γ5, n = 8 (**F**). p-values are shown for

1157 comparisons where a significant difference was observed. Dunn's multiple comparisons

1158 test was performed for all pairwise combinations among γ2-γ5, $p < 0.05$; n = 10 (**D**), γ2-

1159 γ5, $p < 0.05$; n = 10 (**E**) and γ2-γ5, $p < 0.05$; n = 8 (**F**). (**G**) The changes in cAMP (red)

1160 and Dopamine (green) levels over 15-30 seconds in response to different odors (OCT,

1161 MCH, and ACV) in five γ lobe compartments (γ1-γ5). The odors were presented by

1162 opening the solenoid valve between 15-18 seconds. Solid lines represent the average

1163 response from 7 flies, and shaded areas show the standard error of the mean (SEM).

1164 (**H**) Comparison of the odor-evoked calcium responses in the γ2-γ5 compartments

1165 between control and *Dop1R1*$^{KO/KO}$ mutant flies. All values represent the mean ± SEM

1166 values. p-values are shown for comparisons where a significant difference was

1167 observed. Mann-Whitney U test, control: n = 10; *Dop1R1*$^{KO/KO}$*:* n = 8.

1168

Figure 3

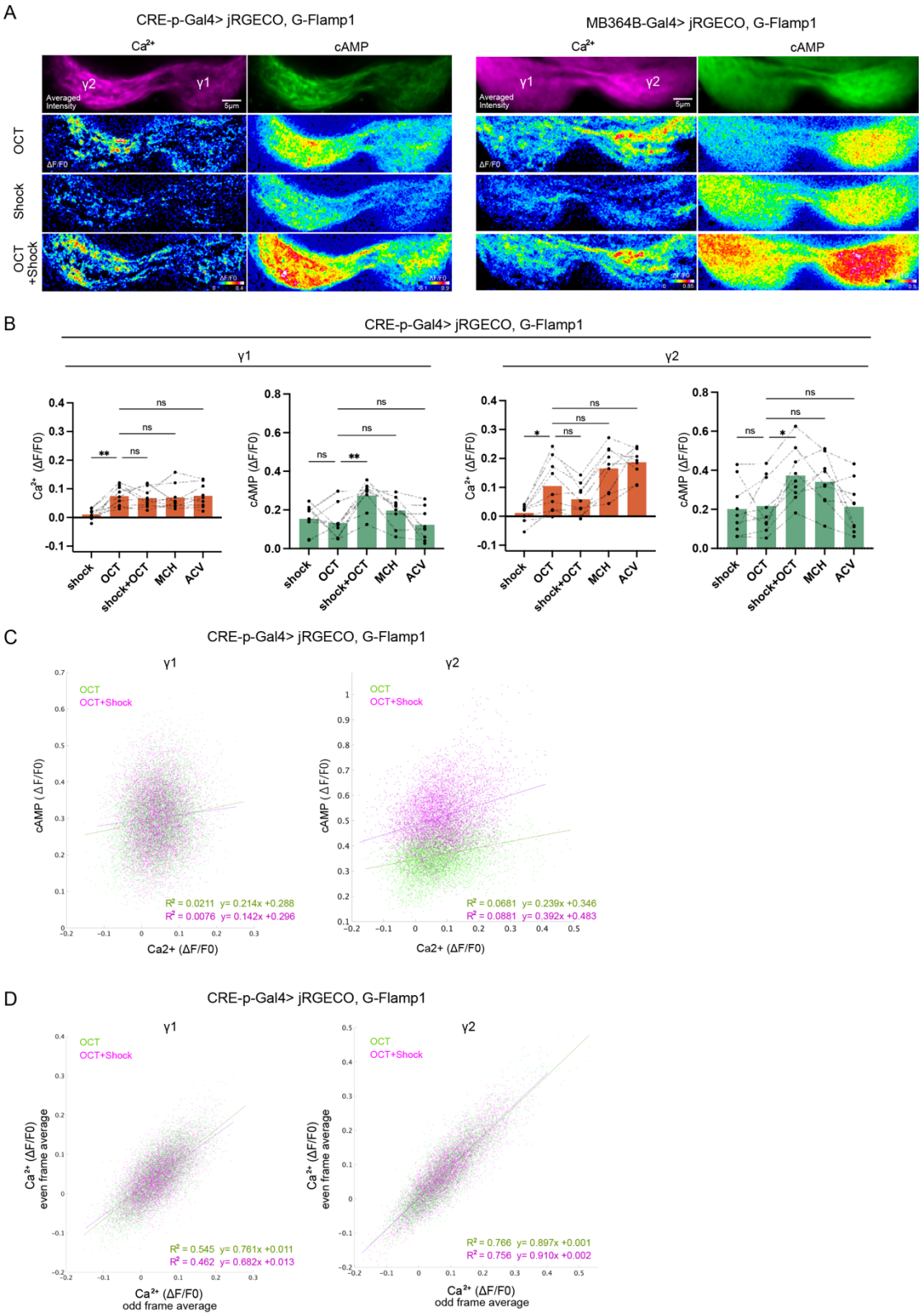

1169

1170 **Figure 3.** cAMP levels are not dependent on calcium levels when odor (CS) and

1171 electric shock (US) are paired. (**A**) The top panels display the averaged

1172 representations of raw intensity values extracted from 80 frames, spanning a duration

1173 of 40 seconds including both stimulus and non-stimulus periods. The following three

1174 panels below present exemplary ΔF/F0 images of averaged peak responses (10

1175 frames, 5 s) of calcium and cAMP during the presentation of OCT, Shock, and both

1176 paired in the γ1-γ2 compartments expressing jRGECO1b and G-Flamp1 driven by the

1177 γCRE-p (left) or MB364B GAL4 (right) driver. (**B**) The averaged ΔF/F0 images of the

1178 γCRE-p flies were quantified. The plots of different stimuli derived from the same

1179 sample are connected with dashed lines. The bar graph illustrates the mean values.

1180 Dunn's multiple comparisons test was conducted using OCT (CS+) stimulation as the

1181 control group to examine differences between the other stimulus groups, *$p < 0.05$, **p

1182 < 0.01, ns, not significant; $n = 9$. (**C**) Scatter plots of ΔF/F0 values derived from

1183 representative averaged calcium and cAMP images of each γ compartment. These

1184 values are derived from the same dataset used in (**B**). The X-axis represents the ΔF/F0

1185 of calcium, while the Y-axis represents the ΔF/F0 of cAMP. The individual points in the

1186 plot correspond to each pixel within the γ1 or γ2 compartment in the averaged ΔF/F0

1187 images, and linear regression lines are plotted. OCT (CS only): green, and OCT +

Shock (CS + US): magenta. (**D**) The X-axis and Y-axis represent the ΔF/F0 of calcium obtained by averaging odd frames and even frames, respectively, from the same calcium imaging data set used in (**C**). The individual points in the plot correspond to each pixel within the γ1 or γ2 compartment, and linear regression lines are plotted. OCT (CS only): green, and OCT + Shock (CS + US): magenta.

Figure 4

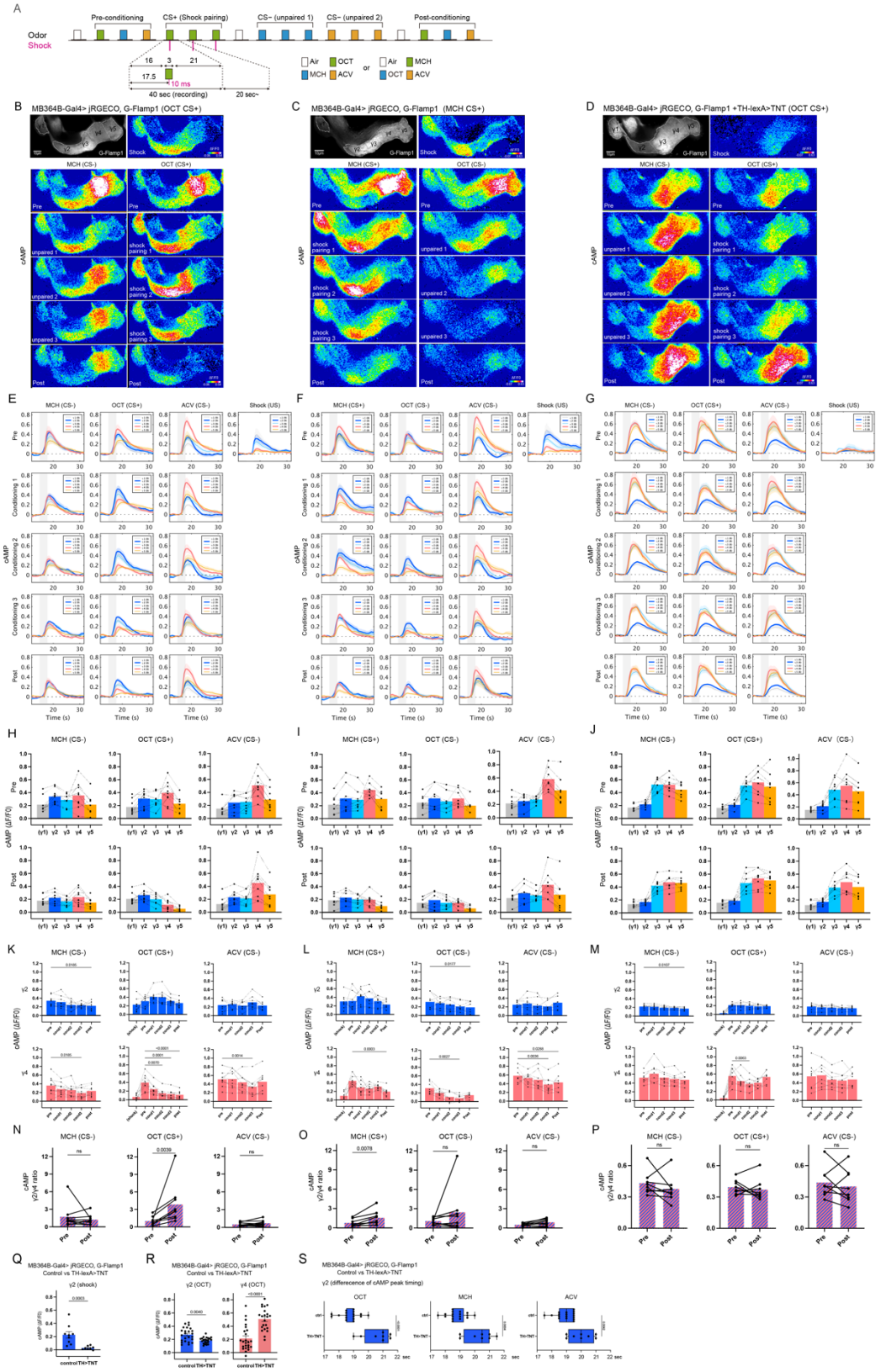
A
Pre-conditioning
CS+ (Shock pairing)
CS− (unpaired 1)
CS− (unpaired 2)
Post-conditioning
Odor
Shock
40 sec (recording)
20 sec~
10 ms
Air
OCT
MCH
ACV
or
B
MB364B-Gal4> jRGECO, G-Flamp1 (OCT CS+)
C
MB364B-Gal4> jRGECO, G-Flamp1 (MCH CS+)
D
MB364B-Gal4> jRGECO, G-Flamp1 +TH-lexA>TNT (OCT CS+)
MCH (CS-)
OCT (CS+)
ACV (CS-)
Shock (US)
cAMP
Pre
Post
Time (s)
cAMP (ΔF/F0)
cAMP γ2/γ4 ratio
MB364B-Gal4> jRGECO, G-Flamp1
Control vs TH-lexA>TNT
γ2 (shock)
γ2 (OCT)
γ4 (OCT)
γ2 (differecence of cAMP peak timing)
OCT
MCH
ACV

1195 **Figure 4.** The cAMP code of an odor is integrated with the cAMP code of an electric

1196 shock during conditioning. (**A**) Schematic representation of conditioning procedure.

1197 Sixteen seconds after the start of the recording, a 3 second odor stimulus was

1198 presented to the fly. Following a delay of 1.5 seconds from the onset of the odor

1199 presentation, an electric shock of 60 volts was administered to the fly for a duration of

1200 10 milliseconds. In one series of experiments, OCT was paired with electric shock,

1201 while MCH and ACV were not (**B and D**). In another set of experiments, MCH was

1202 paired with electric shock, while OCT and ACV were not (**C**). (**B**, **C**, **D**) All the cAMP

1203 images in the γ1-γ5 compartments of KCs were captured from flies expressing G-

1204 Flamp1 and jRGECO1b under the control of the MB364B driver. An averaged raw

1205 intensity image of cAMP derived from 80 frames acquired during air presentation for 40

1206 s, onto which the ROIs for each compartment are mapped (upper left), and the ΔF/F0

1207 image obtained by averaging the responses (5 s, 10 frames) to electric shock (upper

1208 right) are shown. The images displayed below depict the ΔF/F0 images obtained by

1209 averaging the responses (5 s, 10 frames) to OCT (as CS+) during the pre-conditioning,

1210 first, second, and third pairings, as well as post-conditioning. Additionally, the images

1211 illustrate the neural responses to MCH (as CS-) during the same experimental

1212 procedure, but without electric shock (**B**). Similarly, the corresponding images obtained

1213 when MCH was presented as the CS+ and OCT as the CS- are shown in (**C**). In (**D**),
1214 TNT was expressed in PPL1 DANs by the TH-LexA driver to block neurotransmitter
1215 release to innervating compartments. OCT was paired with electric shock, while MCH
1216 and ACV were not, following the same procedure as in (**B**). (**E**, **F**, **G**) A series of line
1217 plots depicting the temporal dynamics of cAMP over time in seconds (s) across
1218 different stimulus conditions. Each subplot corresponds to a different combination of
1219 odor or shock stimulus and time points. Each plot shows the ΔF/F0 of cAMP of the γ1-
1220 γ5 compartments. The solid lines represent the mean values for each compartment,
1221 calculated from the number of flies indicated in parentheses within the subplots. The
1222 shaded areas around each solid line represent the SEM. Shaded rectangular areas
1223 indicate when the odor valve was opened (15 to 18 seconds) to apply the olfactory
1224 stimulus. A 60-volt shock was administered to the fly 17.5 seconds after the start of the
1225 recording, lasting for a duration of 10 milliseconds. (**H**, **I**, **J**) The mean peak ΔF/F0 (10
1226 frames for 5 s) values of each compartment were averaged and represented in bar
1227 graphs, generating cAMP codes for the pre- and post-conditioning responses to each
1228 odor. The plots of different compartments derived from the same sample are
1229 connected with dashed lines. n = 9 (H), 8 (I), and 8 (J). (**K**, **L**, **M**) Dunn's multiple
1230 comparisons test was conducted on the differences in cAMP levels in the γ2 and γ4

1231 compartments, using their pre-odor responses as controls. The same datasets used in

1232 (**H**), (**I**), and (**J**) were utilized for (**K**), (**L**), and (**M**), respectively. The shock values

1233 shown in the (CS+) experimental group were not included in the statistical test. p-

1234 values are shown for comparisons with significant differences. n = 9 (**K**), 8 (**L**), and 8

1235 (**M**). (**N**, **O**, **P**) The ratio of cAMP levels in the γ2 compartment to those in the γ4

1236 compartment for each odor response was calculated. Bar graphs represent mean

1237 values. The ratios obtained before and after the conditioning phase are then compared

1238 by Wilcoxon signed rank test. The same datasets used in (**H**), (**I**), and (**J**) were utilized

1239 for (**N**), (**O**), and (**P**), respectively. p-values are shown for comparisons where a

1240 significant difference was observed. ns, not significant, n = 9 (**N**), 8 (**O**), and 8 (**P**). (**Q**)

1241 Comparison of the electric shock-evoked cAMP responses in the γ2 compartment

1242 between control and TH-lexA>TNT mutant flies. The bar graph represents the mean

1243 values with ± SEM. p-value is shown where a significant difference was observed.

1244 Mann-Whitney U test, control: n = 10; TH-lexA>TNT: n = 8. (**R**) Comparison of the

1245 odor-evoked cAMP responses in the γ2 and γ4 compartments between control and TH-

1246 lexA>TNT mutant flies. The bar graph represents the mean values with ± SEM. p-

1247 values are shown where significant differences were observed. Mann-Whitney U test,

1248 control: n = 10; TH-lexA>TNT: n = 8. (**S**) Comparison of the peak timing of odor-evoked

1249 cAMP responses in the γ2 compartment among control and TH-lexA>TNT mutant flies.

1250 The distributions of the data are represented by box plots, with the whiskers indicating

1251 the minimum and maximum values. p-values are shown where significant differences

1252 were observed. Mann-Whitney U test, control: n = 10; TH-lexA>TNT: n = 8.

1253

Figure 5

CREp-Gal4> Pink Flamindo, GRAB_DA2m

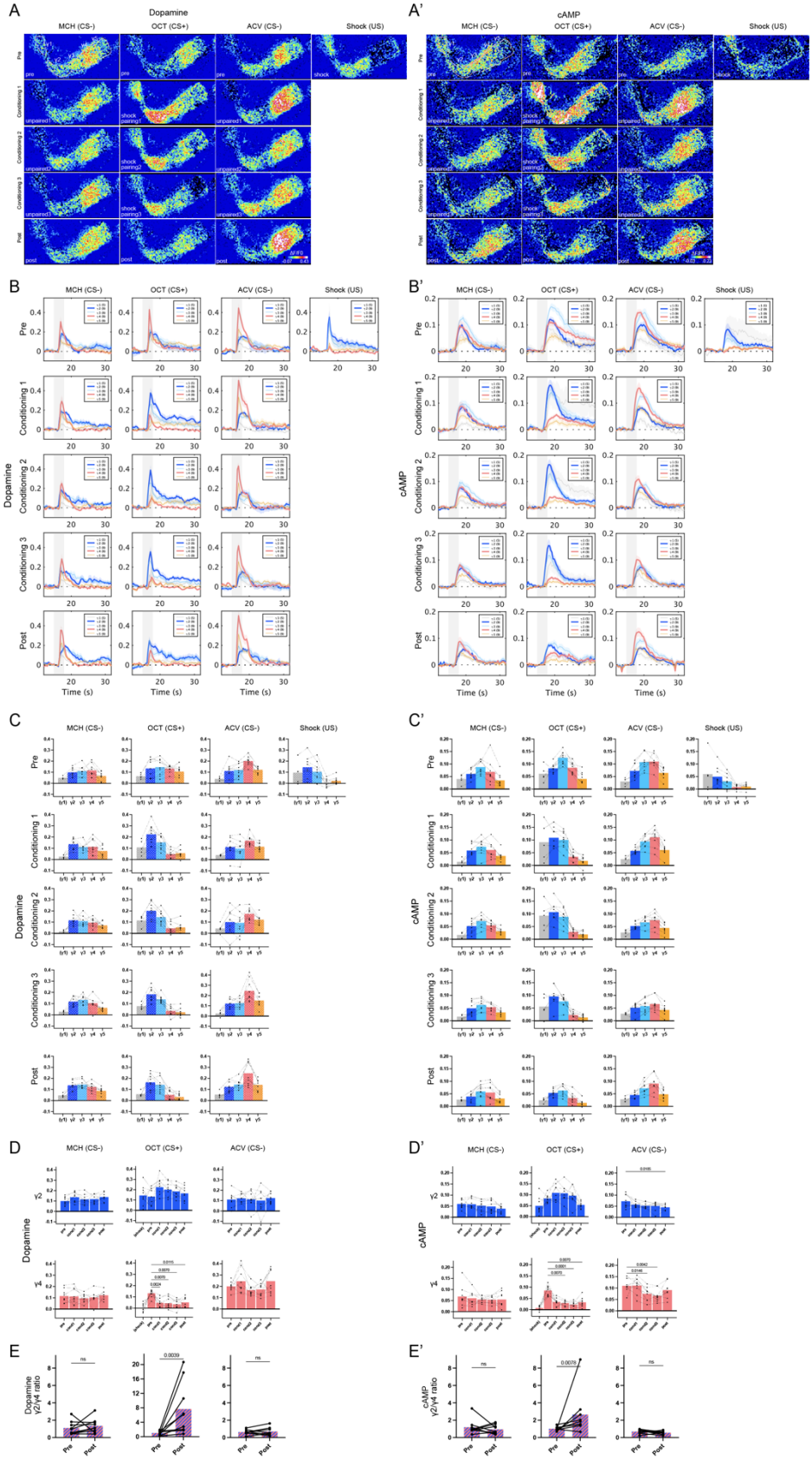

1254

1255 **Figure 5.** Associative conditioning triggers alterations in dopamine levels, leading to
1256 subsequent modifications in the cAMP levels. (**A**, **A'**) The ΔF/F0 images, depicting the
1257 averaged peak responses (15 frames for 5 s) of Dopamine (**A**) and cAMP (**A'**) in the
1258 γ1-γ5 compartments of KCs, were captured from flies expressing Pink Flamindo and
1259 GRAB_DA2m sensors under the control of the γCRE-p driver during the presentations
1260 of OCT (CS+), MCH (CS-), ACV (CS-), and shock (US) through conditioning. The ROIs
1261 for each compartment are mapped onto the top left panel. (**B**, **B'**) A series of line plots
1262 depicting the temporal dynamics of Dopamine (**B**) and cAMP (**B'**) over time in seconds
1263 (s) across different stimulus conditions. Each subplot corresponds to a different
1264 combination of odor or shock stimulus and time points. The y-axis indicates ΔF/F0. The
1265 solid lines represent the mean values for each compartment, calculated from the
1266 number of flies indicated in parentheses within the subplots. The shaded areas around
1267 each line represent the SEM. Shaded rectangular areas indicate when the odor valve
1268 was opened (15 to 18 seconds) to apply the olfactory stimulus. A 60-volt shock was
1269 administered to the fly 17.5 seconds after the start of the recording, lasting for a
1270 duration of 10 milliseconds. (**C**, **C'**) Quantifications of the ΔF/F0 images of cAMP (left)
1271 and ACh (right) obtained by averaging the pre- and post-conditioning responses to
1272 odors and shock. The plots of different compartments derived from the same sample

are connected with dashed lines. The bar graph illustrates the mean values. (**D**, **D’**) Dunn’s multiple comparisons test was conducted on the differences in Dopamine (**D**) and cAMP (**D’**) levels in the γ2 and γ4 compartments, using their pre-odor responses as controls. The same datasets used in (**C**) and (**C’**) were utilized for (**D**) and (**D’**), respectively. The shock values shown in the (CS+) experimental group were not included in the statistical test. p-values are shown for comparisons with significant differences. n = 9 for all stimulus sets in both γ2 and γ4. (**E**, **E’**) Comparisons of the γ2/4 Dopamine ratio before and after the conditioning phase for each odor (**E**). Similarly, the γ2/4 cAMP ratios before and after the conditioning phase are compared (**E’**). The same datasets used in (**C**) and (**C’**) were utilized for (**E**) and (**E’**), respectively. p-values are shown for comparisons where a significant difference was observed. ns, not significant, n = 9, 9, 8 (**E**), and 9, 9, 9 (**E’**). Wilcoxon signed rank test.

Figure 6

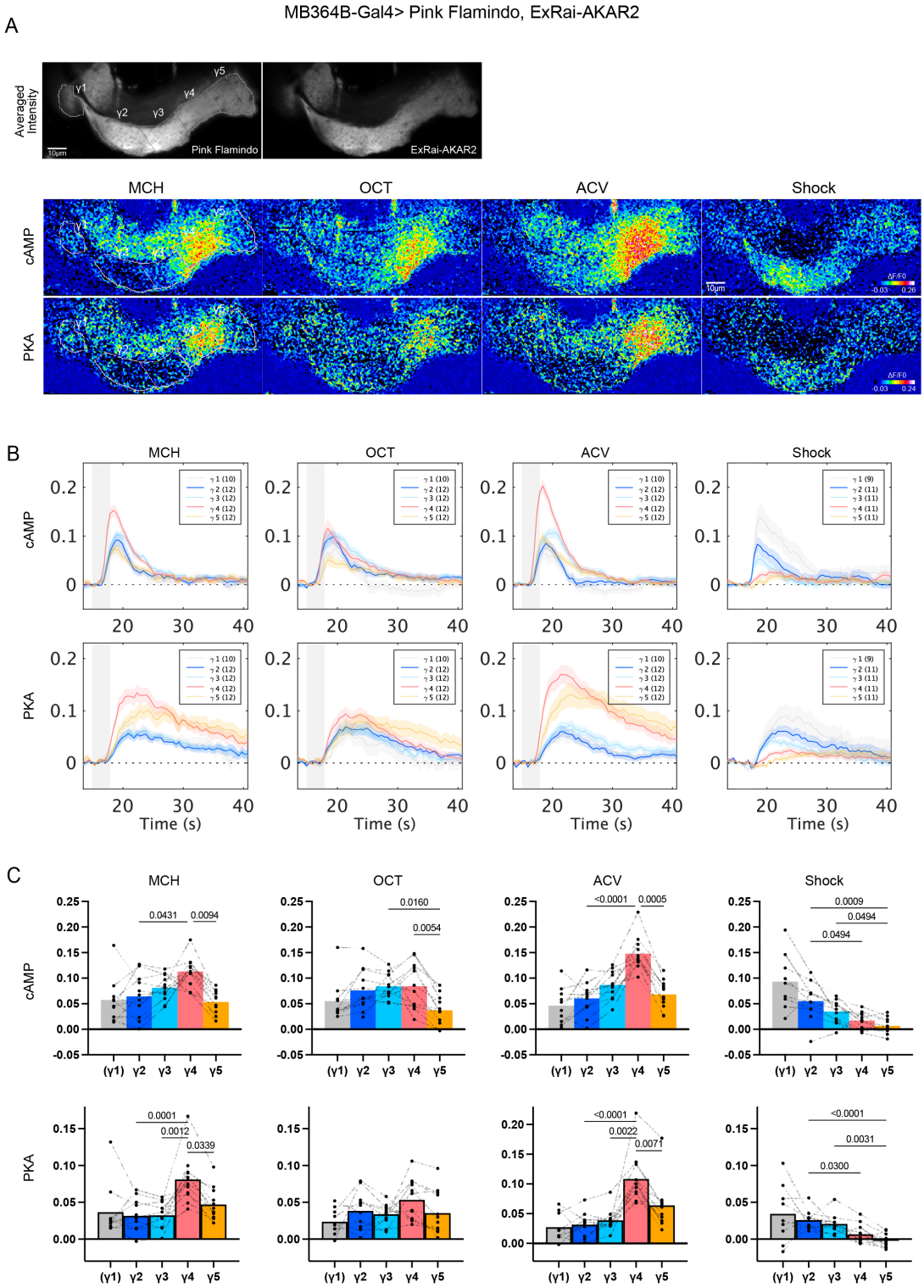

Figure 6. The protein kinase A (PKA) activities coincide with the presence of cAMP.

(**A**) The top two panels display the averaged representations of raw intensity values extracted from 120 frames, spanning a duration of 60 seconds, including both stimulus and non-stimulus periods, in flies expressing Pink Flamindo for cAMP detection and ExRai-AKAR2 for PKA activity detection under the control of the MB364B-GAL4 driver. The ROIs for each compartment are mapped onto the top left panel. The following eight panels show the mean peak ΔF/F0 images obtained by averaging each response (5 s, 10 frames) in the γ1-γ5 compartments during OCT, MCH, ACV, and shock presentation. (**B**) A series of line plots depicting the temporal dynamics of cAMP (upper panels) and PKA (lower panels) over time in seconds (s) across different stimulus conditions. Each subplot corresponds to a different combination of odor or shock stimulus and time points. The y-axis indicates ΔF/F0. The solid lines represent the mean values for each compartment, calculated from the number of flies indicated in parentheses within the subplots. The shaded areas around each line represent the SEM. Shaded rectangular areas indicate when the odor valve was opened (15 to 18 seconds) to apply the olfactory stimulus. A 60-volt shock was administered to the fly 17.5 seconds after the start of the recording, lasting for a duration of 10 milliseconds. (**C**) Quantification of the averaged peak ΔF/F0 images (10 frames for 5 s) of cAMP (upper panels) and PKA activity (lower panels). The plots of different compartments

derived from the same sample are connected by dashed lines. The bar graph represents the mean values. Dunn's multiple comparisons test was conducted for all pairwise combinations among γ2-γ5. p-values are shown for comparisons with significant differences, n = 12 for all data sets.

Figure 7

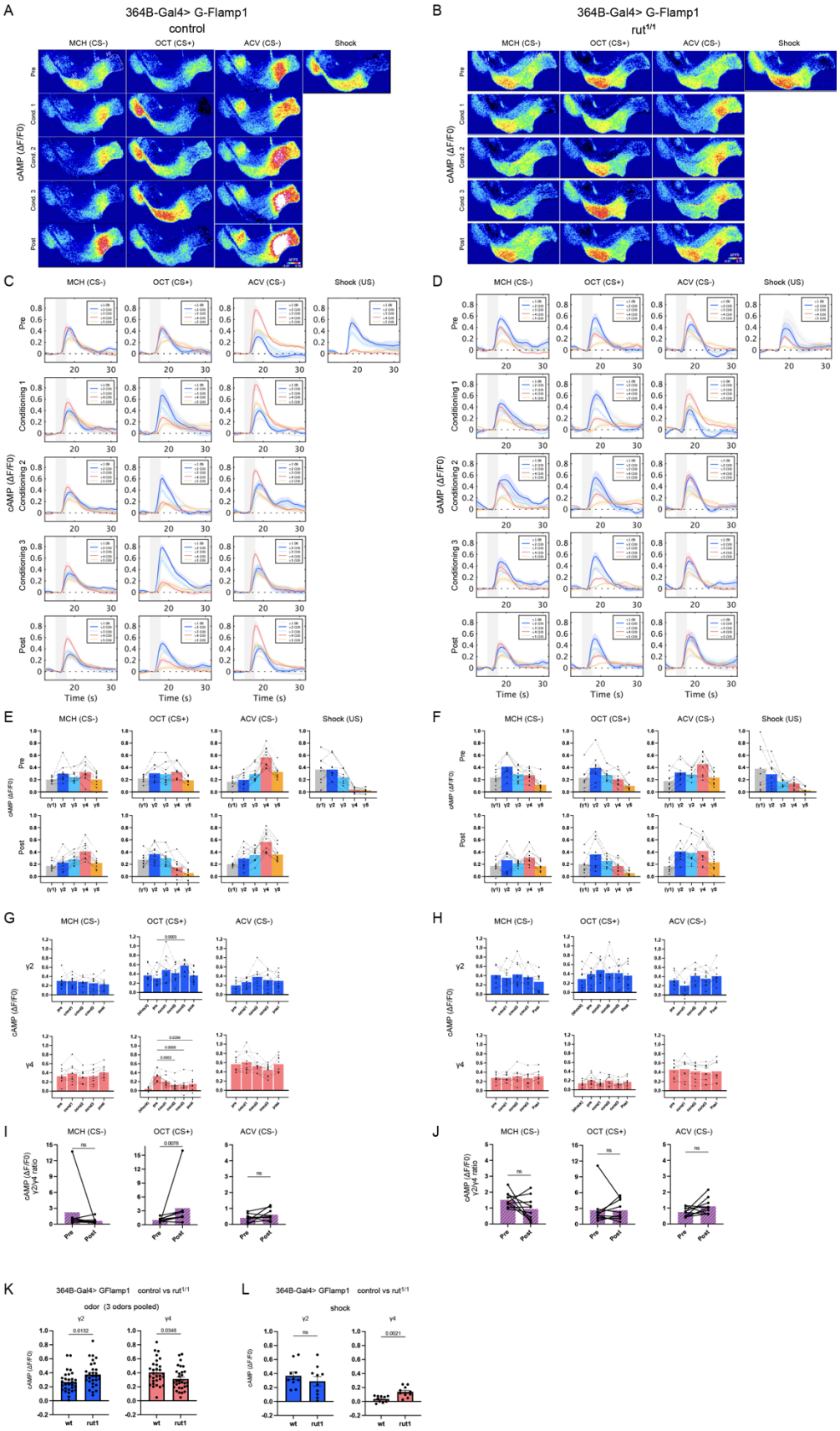
A
364B-Gal4> G-Flamp1
control
B
364B-Gal4> G-Flamp1
rut1/1
MCH (CS-)
OCT (CS+)
ACV (CS-)
Shock
Pre
Cond. 1
Cond. 2
Cond. 3
Post
cAMP (ΔF/F0)
C
D
Shock (US)
Conditioning 1
Conditioning 2
Conditioning 3
Time (s)
E
F
G
H
γ2
γ4
I
J
cAMP (ΔF/F0) γ2/γ4 ratio
K
364B-Gal4> GFlamp1 control vs rut1/1
odor (3 odors pooled)
L
shock
wt
rut1

1312 **Figure 7.** Distinct cAMP codes between control and $rut^{1/1}$ mutant flies.

1313 (**A, B**) The ΔF/F0 images, showing the averaged peak responses (10 frames over 5 s)

1314 of cAMP in the γ1-γ5 compartments of KCs, were captured during the presentations of

1315 OCT (CS+), MCH (CS-), ACV (CS-), and shock (US) in the genetic control fly (**A**) and

1316 $rut^{1/1}$ mutant fly (**B**) through the conditioning. The ROIs for each compartment are

1317 mapped onto the top left panel. (**C**, **D**) The figure represents a series of line plots

1318 depicting the temporal dynamics of cAMP over time in seconds (s) across different

1319 stimulus conditions. Each subplot corresponds to a different combination of odor or

1320 shock stimulus and time points. Each plot shows the ΔF/F0 of cAMP of the γ1-γ5

1321 compartments. The solid lines represent the mean values for each compartment,

1322 calculated from the number of flies indicated in parentheses within the subplots. The

1323 shaded areas around each solid line represent the SEM. Shaded rectangular areas

1324 indicate when the odor valve was opened (15 to 18 seconds) to apply the olfactory

1325 stimulus. During the conditioning, the cAMP increase in the γ2 compartment or the

1326 decrease in the γ4 and 5 compartments in the rut^{1} mutant (**D**, OCT CS+ lanes) was

1327 much less pronounced than in the control group (**C**, OCT CS+ lane). (**E**, **F**)

1328 Quantification of the averaged ΔF/F0 images of control (**E**) and $rut^{1/1}$ (**F**) flies. The plots

1329 of different compartments derived from the same sample are connected with dashed

1330 lines. The bar graph represents the mean values. γ1: n = 9, γ2-γ5: n = 10 (**E**), and γ1: n

1331 = 9, γ2-γ5: n = 10 (**F**). (**G**, **H**) Dunn's multiple comparisons test was conducted on the

1332 differences in cAMP levels in the γ2 and γ4 compartments on control (**G**) and $rut^{1/1}$ (**H**)

1333 flies, using their pre-odor responses as controls. The same datasets used in (**E**) and

1334 (**F**) were utilized for (**G**) and (**H**), respectively. The shock values shown in the (CS+)

1335 experimental group were not included in the statistical test. p-values are shown for

1336 comparisons with significant differences. n = 10 for all stimulus sets in both γ2 and γ4.

1337 (**I**, **J**) The ratio of cAMP levels in the γ2 compartment to those in the γ4 compartment

1338 for each odor response was calculated. Bar graphs represent mean values. The ratios

1339 obtained before and after the conditioning phase are compared by the Wilcoxon signed

1340 rank test. The same datasets used in (**E**) and (**F**) were utilized for (**I**) and (**J**),

1341 respectively. Unlike the control, the γ2/4 ratio of the OCT (CS+) response of $rut^{1/1}$

1342 remained unchanged between pre- and post-response. p-values are shown for

1343 comparisons where a significant difference was observed. ns, not significant, n = 9 (**I**)

1344 and 10 (**J**). (**K**) Comparison of the odor-evoked cAMP responses in the γ2 and γ4

1345 compartments between control and $rut^{1/1}$ mutant flies. The bar graph represents the

1346 mean values with ± SEM. p-values are shown where significant differences were

1347 observed. Mann-Whitney U test, control: n = 30; $rut^{1/1}$: n = 30. (**L**) Comparison of the

1348 electric shock-evoked cAMP responses in the γ2 and γ4 compartments between

1349 control and $rut^{1/1}$ mutant flies. The bar graph represents the mean values with ± SEM.

1350 p-value is shown where a significant difference was observed. ns, not significant,

1351 Mann-Whitney U test, control: n = 10; $rut^{1/1}$: n = 10.

1352

Figure 8

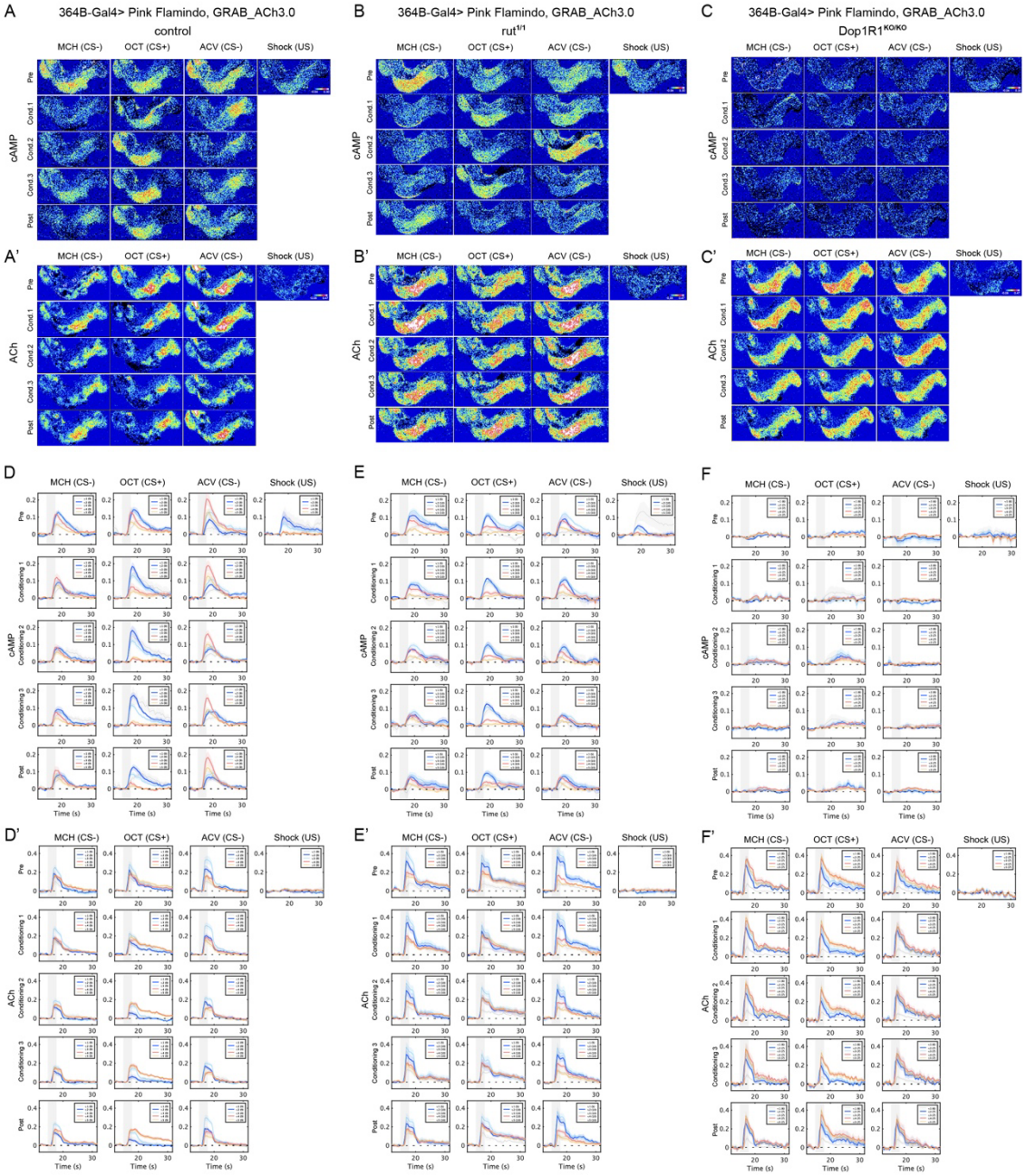

1353

1354

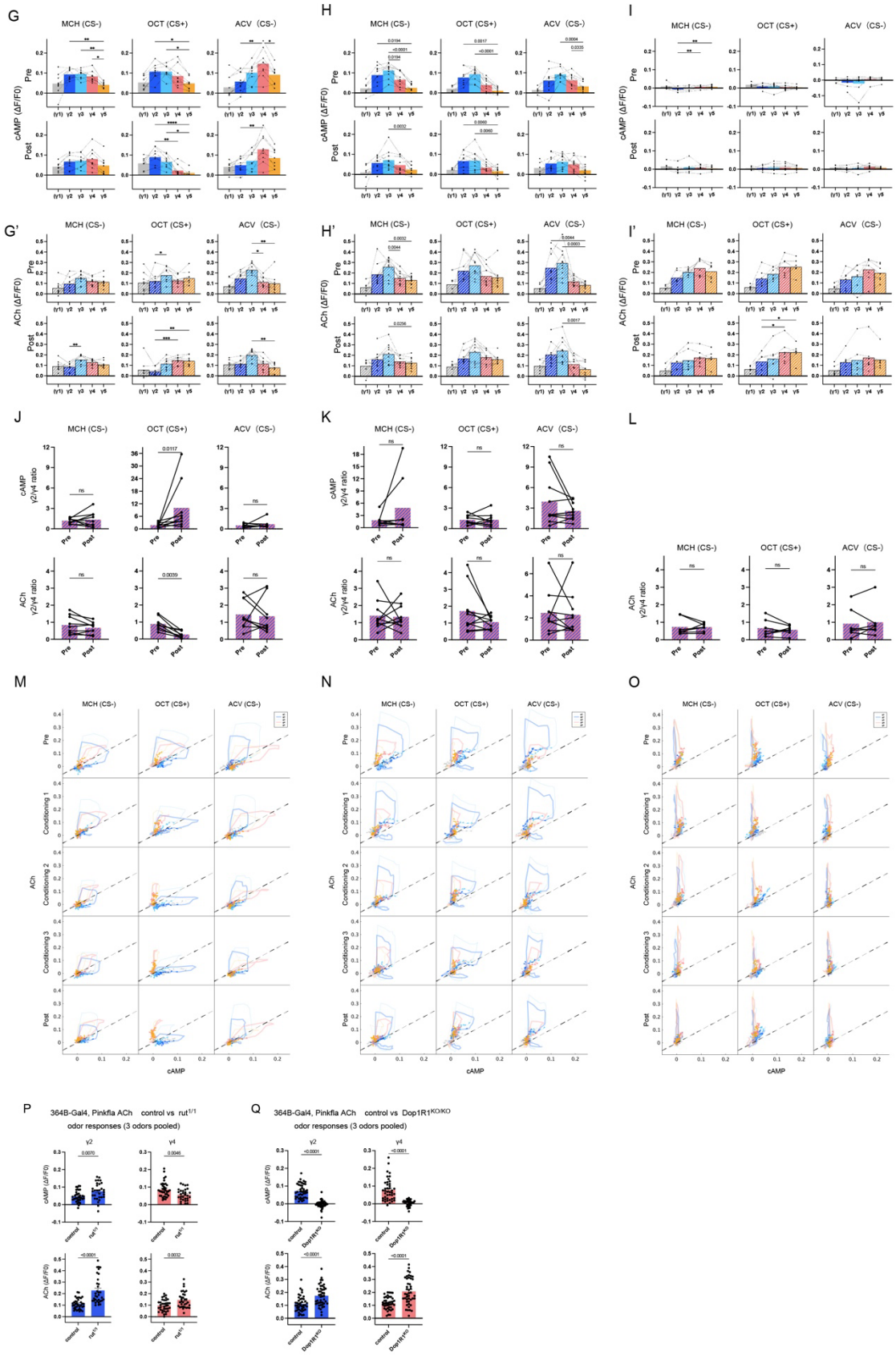
G
H
I
G'
H'
I'
J
K
L
M
N
O
P
Q
MCH (CS-)
OCT (CS+)
ACV (CS-)
cAMP (ΔF/F0)
ACh (ΔF/F0)
Pre
Post
cAMP γ2/γ4 ratio
ACh γ2/γ4 ratio
Conditioning 1
Conditioning 2
Conditioning 3
cAMP
ACh
364B-Gal4, Pinkfla ACh control vs rut1/1
odor responses (3 odors pooled)
364B-Gal4, Pinkfla ACh control vs Dop1R1KO/KO
odor responses (3 odors pooled)
γ2
γ4
control

1356 **Figure 8.** Acetylcholine release is inversely correlated with cAMP levels following
1357 conditioning. All the cAMP and ACh images in the γ1-γ5 compartments of KCs were
1358 simultaneously captured from flies expressing Pink Flamindo and GRAB_ACh3.0
1359 under the control of the MB364B-GAL4 driver and subjected to aversive conditioning,
1360 following the procedure outlined in Figure 4. (**A**, **A'**, **B**, **B'**, **C**, **C'**) The ΔF/F0 images,
1361 depicting the averaged peak responses (10 frames for 5 s) of cAMP (**A, B, C**) and ACh
1362 (**A'**, **B'**, **C'**) in the γ1-γ5 compartments of KCs, were captured during the presentations
1363 of OCT (CS+), MCH (CS-), ACV (CS-) and shock (US) through the conditioning in
1364 control, $rut^{1/1}$ mutant, and $Dop1R1^{KO/KO}$ mutant flies, respectively. The ROIs for each
1365 compartment are mapped onto the top left panel. (**D**, **D'**, **E**, **E'**, **F**, **F'**) A series of line
1366 plots depicting the temporal dynamics of simultaneously recorded AMP and ACh over
1367 time in seconds (s) across different stimulus conditions. Each subplot corresponds to a
1368 different combination of odor or shock stimulus and time points. Each plot shows the
1369 ΔF/F0 of cAMP (**D**, **E**, **F**) and ACh (**D'**, **E'**, **F'**) of the γ1-γ5 compartments. The solid
1370 lines represent the mean values for each compartment, calculated from the number of
1371 flies indicated in parentheses within the subplots. The shaded areas around each solid
1372 line represent the SEM. Shaded rectangular areas indicate when the odor valve was
1373 opened (15 to 18 seconds) to apply the olfactory stimulus. A 60-volt shock was

1374 administered to the fly 17.5 seconds after the start of the recording, lasting for a

1375 duration of 10 milliseconds. (**G**, **G'**, **H**, **H'**, **I**, **I'**) The averaged peak ΔF/F0 images of the

1376 pre- and post-conditioning responses to odors were quantified. (**G**, **H**, **I**) represent

1377 cAMP, while (**G'**, **H'**, **I'**) represent ACh. The plots of different compartments derived

1378 from the same sample are connected with dashed lines. The bar graph illustrates the

1379 mean values. p-values are shown for comparisons with significant differences. Dunn's

1380 multiple comparisons test for all pairwise combinations among γ2-γ5. n = 9 (**G**,**G'**), n =

1381 10 (**H**, **H'**), and n = 7 (**I**, **I'**). (**J**, **K**, **L**) For calculating the γ2/γ4 ratio, the same datasets

1382 used in (**G-G'**, **H-H'**, **I-I'**) were utilized for (**J**), (**K**), (**L**), respectively. The ratios obtained

1383 before and after the conditioning phase were compared by the Wilcoxon signed rank

1384 test. The γ2/4 ratios of cAMP before and after the conditioning phase for each odor are

1385 represented in the upper panels. We did not calculate the cAMP ratio for the

1386 Dop1R1$^{KO/KO}$ mutant because the putative averaged peak ΔF/F0 was often negative in

1387 the γ2 or γ4 compartment in several trials (see **I**). The γ2/4 ratios of ACh before and

1388 after the conditioning phase for each odor (lower panels in **J**, **K**, **L**) were also

1389 compared. p-values are shown for comparisons where a significant difference was

1390 observed. Unlike the control, no statistically significant differences in the γ2/γ4 cAMP

1391 ratios between pre- and post-conditioning specific to CS+ were detected in the rut$^{1/1}$

1392 mutant: n = 9, 9, 7 in (**J**) and n =8, 10, 9 in (**K**). Similarly, no statistically significant

1393 differences in the γ2/γ4 ACh ratios between pre and post specific to CS+ were

1394 detected in both the $rut^{1/1}$ mutant and the Dop1R1 mutant: n = 9, 9, 9 in (**J**), n = 10, 10,

1395 10 in (**K**), and n = 7, 7, 7 in (**L**). ns, not significant. (**M**, **N**, **O**) The relationship between

1396 the changes in cAMP and ACh under different conditions and the time points. Each

1397 subplot illustrates the trajectories of cAMP and ACh ΔF/F0 values over time for the γ1-

1398 γ5 compartments. The values at each point along the trajectories were derived by

1399 averaging the individual data from the same dataset used for (**D-F'**). The trajectories in

1400 (**M**) used the dataset from (**D**, **D'**), (**N**) used the dataset from (**E**, **E'**), and (**O**) used the

1401 dataset from (**F**, **F'**). (**P**) Comparison of the odor-evoked cAMP responses in the γ2 and

1402 γ4 compartments between control and $rut^{1/1}$ mutant flies. The bar graph represents the

1403 mean values with ± SEM. p-values are shown where significant differences were

1404 observed. Mann-Whitney U test, control: n = 36 (MCH: 12, OCT: 12, ACV: 12) and

1405 $rut^{1/1}$: n = 30 (MCH: 10, OCT: 10, ACV: 10). (**Q**) Comparison of the odor-evoked cAMP

1406 responses in the γ2 and γ4 compartments between control and $Dop1R1^{KO/KO}$ mutant

1407 flies. The bar graph represents the mean values with ± SEM. p-values are shown

1408 where significant differences were observed. Mann-Whitney U test, control: n = 42

1409 (MCH: 12, OCT: 12, ACV: 12) and $rut^{1/1}$: n = 45 (MCH: 15, OCT: 15, ACV: 15).

Figure 9

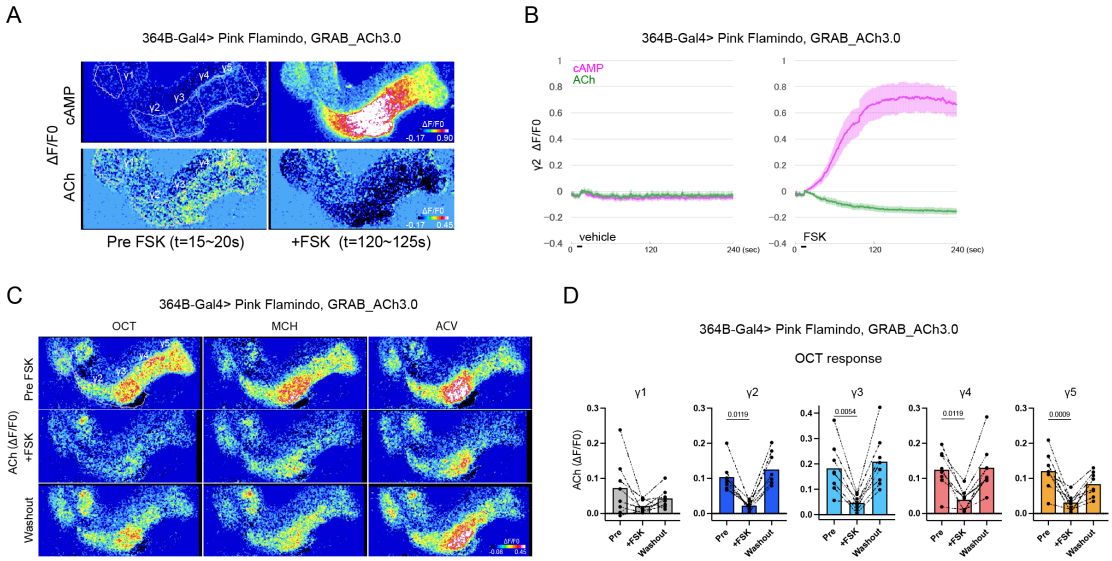

Figure 9. cAMP depresses ACh release from KCs. The release of ACh by activating adenylyl cyclase through the bath application of Forskolin was monitored in flies expressing Pink Flamindo and GRAB_ACh3.0 under the control of the MB364B-GAL4 driver. (**A**) The ΔF/F0 images of cAMP and ACh were obtained by averaging the responses (10 frames for 5 s) immediately after pre FSK (left panels) and 2 minutes after + FSK (right panels) switching from standard saline to saline containing 100 μM Forskolin. The ROIs for each compartment are mapped onto the top left panel. (**B**) The time series traces of cAMP (magenta) and ACh (green) illustrate the changes in their levels after switching to the vehicle (left) and to saline containing 100 μM Forskolin (right). The line and shading represent the mean ± SEM. n = 8. (**C**) ΔF/F0 images of averaged peak responses (10 frames for 5 s) of ACh during the presentation of OCT, MCH, or ACV, each in standard saline (Pre FSK), four minutes after transitioning to

1423 saline containing 100 μM Forskolin (+ FSK), and following the reintroduction of

1424 standard saline (Washout). The ROIs for each compartment are mapped onto the top

1425 left panel. (**D**) The averaged peak ΔF/F0 responses of ACh to OCT in pre-Forskolin,

1426 +Forskolin, and Washout conditions, as depicted in (**C**), were quantified for each

1427 compartment. The plots of different conditions derived from the same sample are

1428 connected with dashed lines. The bar graph illustrates the mean values. The Dunn's

1429 multiple comparisons test was conducted using the Pre FSK OCT response as the

1430 control group to examine differences between the other stimulus groups. p-values are

1431 shown where significant differences were observed. γ1-γ5; n = 8.

1432

Figure 10

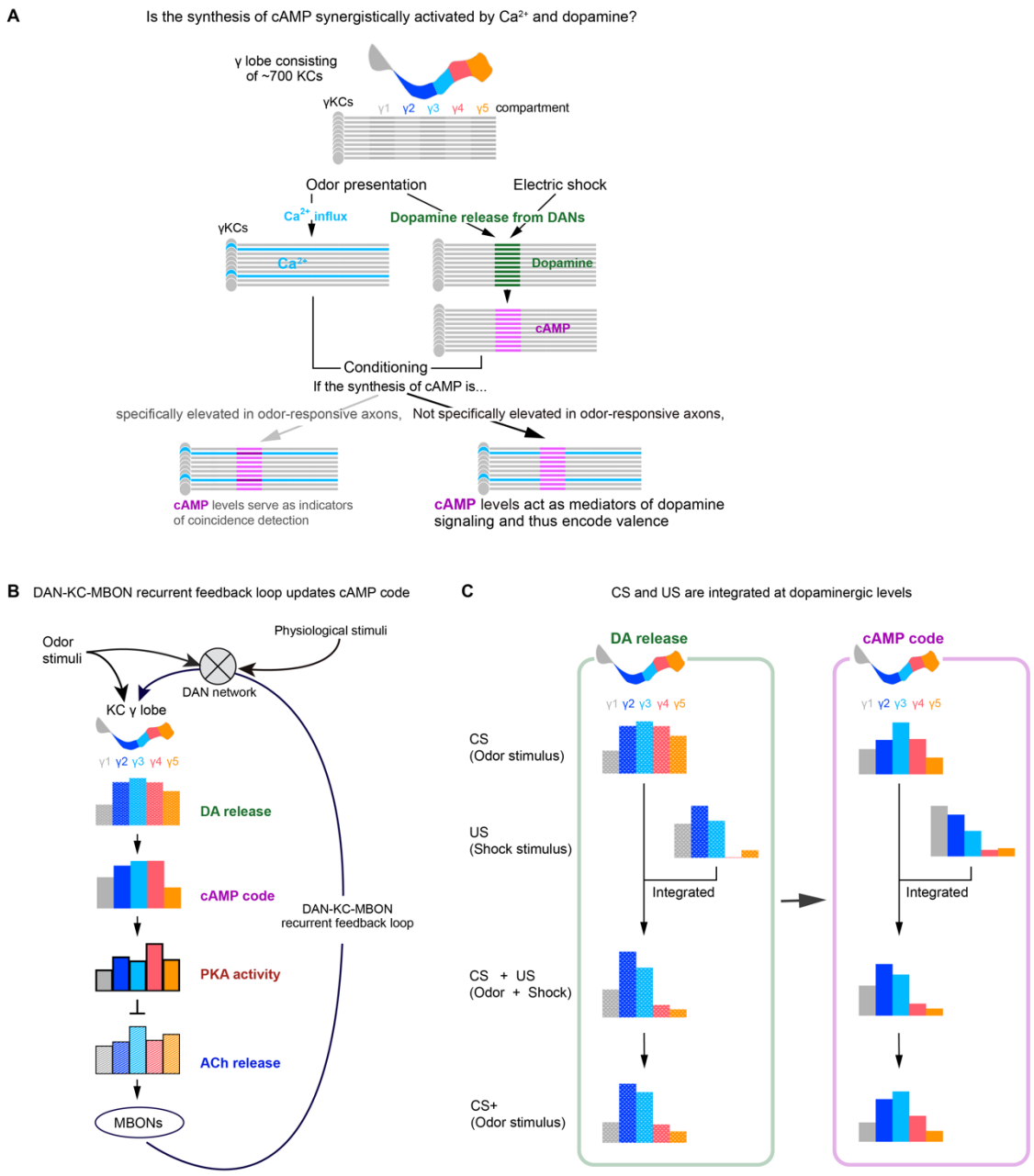
A
Is the synthesis of cAMP synergistically activated by Ca2+ and dopamine?
γ lobe consisting of ~700 KCs
γKCs
γ1 γ2 γ3 γ4 γ5 compartment
Odor presentation
Electric shock
Ca2+ influx
Dopamine release from DANs
γKCs
Ca2+
Dopamine
cAMP
Conditioning
If the synthesis of cAMP is...
specifically elevated in odor-responsive axons,
Not specifically elevated in odor-responsive axons,
cAMP levels serve as indicators of coincidence detection
cAMP levels act as mediators of dopamine signaling and thus encode valence
B
DAN-KC-MBON recurrent feedback loop updates cAMP code
Odor stimuli
Physiological stimuli
DAN network
KC γ lobe
γ1 γ2 γ3 γ4 γ5
DA release
cAMP code
DAN-KC-MBON recurrent feedback loop
PKA activity
ACh release
MBONs
C
CS and US are integrated at dopaminergic levels
DA release
cAMP code
γ1 γ2 γ3 γ4 γ5
CS (Odor stimulus)
US (Shock stimulus)
Integrated
CS + US (Odor + Shock)
CS+ (Odor stimulus)

1434 **Figure 10.** (**A**) Does cAMP serve as a marker for coincidence detection? The γ lobe
1435 comprises approximately 700 Kenyon cells (KCs) and is partitioned into five
1436 compartments, and each receives its own distinct dopaminergic innervation. Each
1437 olfactory stimulus elicits calcium transients in a unique subset of approximately 5% of
1438 KCs and activates a specific subset of the dopaminergic neurons. Consequently, KCs
1439 receive compartment-specific dopamine signals along the entire length of the lobe,
1440 exhibiting distinct characteristics for each odor. The release of dopamine occurs
1441 through volume transmission, leading to its detection in a population of axons that
1442 spans nearly the entire breadth of the lobe. For simplicity, only the dopamine signal
1443 within the γ2 compartment is depicted. This detection roughly coincides with the
1444 presence of cAMP. If the synthesis of cAMP is significantly enhanced by calcium, then
1445 the axons of odor-responsive KCs with high calcium signals exhibit elevated cAMP
1446 synthesis. Conversely, if calcium does not predominantly regulate cAMP synthesis,
1447 then the axons activated by olfactory stimuli are not distinguished by their cAMP levels.
1448 Our findings corroborate the latter hypothesis and indicate that cAMP serves as a
1449 mediator of the dopamine signal. **(B)** DAN-KC-MBON recurrent feedback loop updates
1450 cAMP code. cAMP levels in each compartment depend on receiving dopamine
1451 conveying negative valence to the γ1-3 compartments and positive valence to the γ4-5

compartments. The global equilibrium of cAMP levels throughout the γ lobe could yield a comprehensive depiction of the integrated valence, which can be portrayed as a two-dimensional image of cAMP levels and designated as the cAMP code. KCs exert regulatory control over the functions of their downstream targets; namely, the mushroom body output neurons (MBONs), through the release of acetylcholine (ACh). cAMP serves as a negative regulator of ACh release through the activity of PKA. In turn, the MBONs reciprocally modulate dopaminergic activities, thereby establishing a complex DAN-KC-MBON recurrent feedback loop. The responses to octanol presentations are derived from Figures 5 (dopamine), 6 (cAMP and PKA) and 8 (Ach), and subsequently normalized. **(C)** CS and US are integrated at dopaminergic levels. When the odor is associated with electric shock, the dopaminergic levels in the γ2 compartment increase while those in the γ4 compartment decrease, a pattern that is subsequently reflected in the cAMP code. This indicates that conditioned stimulus (odor) and unconditioned stimulus (electric shock) are integrated at the dopaminergic levels. The responses to octanol and shock presentations are derived from Figure 5.